



Generalized Analysis-oriented model of FRP confined concrete circular columns



Javad Shayanfar^{a,*}, Joaquim A.O. Barros^b, Mohammadali Rezazadeh^c

^a ISISE, Department of Civil Engineering, University of Minho, Azurém 4800-058, Guimarães, Portugal

^b ISISE, IBS, Department of Civil Engineering, University of Minho, Azurém 4800-058, Guimarães, Portugal

^c Civil Eng., Department of Mechanical and Construction Engineering, Northumbria University, Newcastle upon Tyne NE1 8ST, United Kingdom

ARTICLE INFO

Keywords:

FRP confined columns
FRP confinement
Axial behavior
Dilation behavior
Confinement stiffness index

ABSTRACT

This study is dedicated to the development of a generalized confinement model applicable to circular concrete columns confined by FRP full and partial confinement arrangements. To simulate the axial stress versus strain curve, a new strength model is proposed addressing the relation of axial stress and confinement pressure during axial loading, whose calibration was based on an extensive set of test results. By combining theoretical basis and experimental observations, the influence of non-homogenous distribution of concrete transversal expansibility with full/partial confinement during axial compressive loading is taken into the account in the establishment of confinement stiffness index. To estimate the ultimate condition of FRP fully/partially confined concrete, a new model with a design framework is also developed. It is demonstrated that global axial stress–strain curves and also dilation responses simulated by the proposed confinement model are in good agreement with those registered experimentally in available literature, and provides better predictions in terms of ultimate axial stress/strain than the formulations proposed by design standards.

1. Introduction

The reliability of fiber-reinforced-polymer (FRP) composites in various axial/shear/flexural strengthening scenarios has been demonstrated at laboratory level, as well as in real case applications in order to retrofit vulnerable as-built RC columns over seismic actions. For the case of axial strengthening, based on numerous experimentally, numerically, and theoretically conducted studies, it is now well-established that the application of FRP lateral confinement arrangements is efficiently capable of inducing improvements in terms of axial strength and deformability due to the curtailment of concrete lateral expansibility.

An experimental study conducted by Oliveira *et al.* [1] revealed that the capability of confinement strategy for improving the axial response of FRP fully confined concrete columns (FFC as illustrated in Fig. 1) is a function of the type of FRP material, concrete compressive strength, and confinement stiffness, which was also confirmed by Lim and Ozbakkaloglu [2–4]. Zeng *et al.* [5] have experimentally evaluated the efficiency of partial confinement arrangements using carbon fiber-reinforced polymer (CFRP) for increasing the load carrying capacity of concrete columns. The test results demonstrated that the

axial and dilation responses of FRP partially confined concrete columns (FPC as illustrated in Fig. 1) strongly depend on the distance between consecutive strips (s_f) as a key parameter, besides the strip thickness and width, and the used FRP material properties. Barros and Ferreira [6] evidenced that by increasing s_f , the axial and dilation responses of FPC drove to be similar to those of unconfined concrete (UC), as verified by Zeng *et al.* [7]. For the case of FPC, Guo *et al.* [8,9] and Janwaen *et al.* [10,11] showed that concrete at the middle distance between two consecutive FRP strips, known as critical section, would be subjected to the maximum transversal deformation in comparison with the concrete expansion at the strip regions.

Numerous confinement models, known as analysis-oriented model (i.e. [3,12–15]), have been proposed to simulate global axial stress–strain of FFC. Based on the implemented methodology for the establishment of axial stress–strain relationship, these models can be generally classified into three categories as demonstrated in Table 1. Category I (i.e. Lim and Ozbakkaloglu [15]) includes models for actively confined concrete columns (AFC), where the concrete is subjected to an active confinement pressure (f_l^{Active}), with a constant value during entire axial loading, as illustrated in Fig. 1b. In this case, axial stress (f_c^{Active}) at a certain axial strain (ϵ_c) can be determined by adopt-

* Corresponding author.

E-mail addresses: jd8287@alunos.uminho.pt (J. Shayanfar), barros@civil.uminho.pt (J.A.O. Barros), mohammadali.rezazadeh@northumbria.ac.uk (M. Rezazadeh).

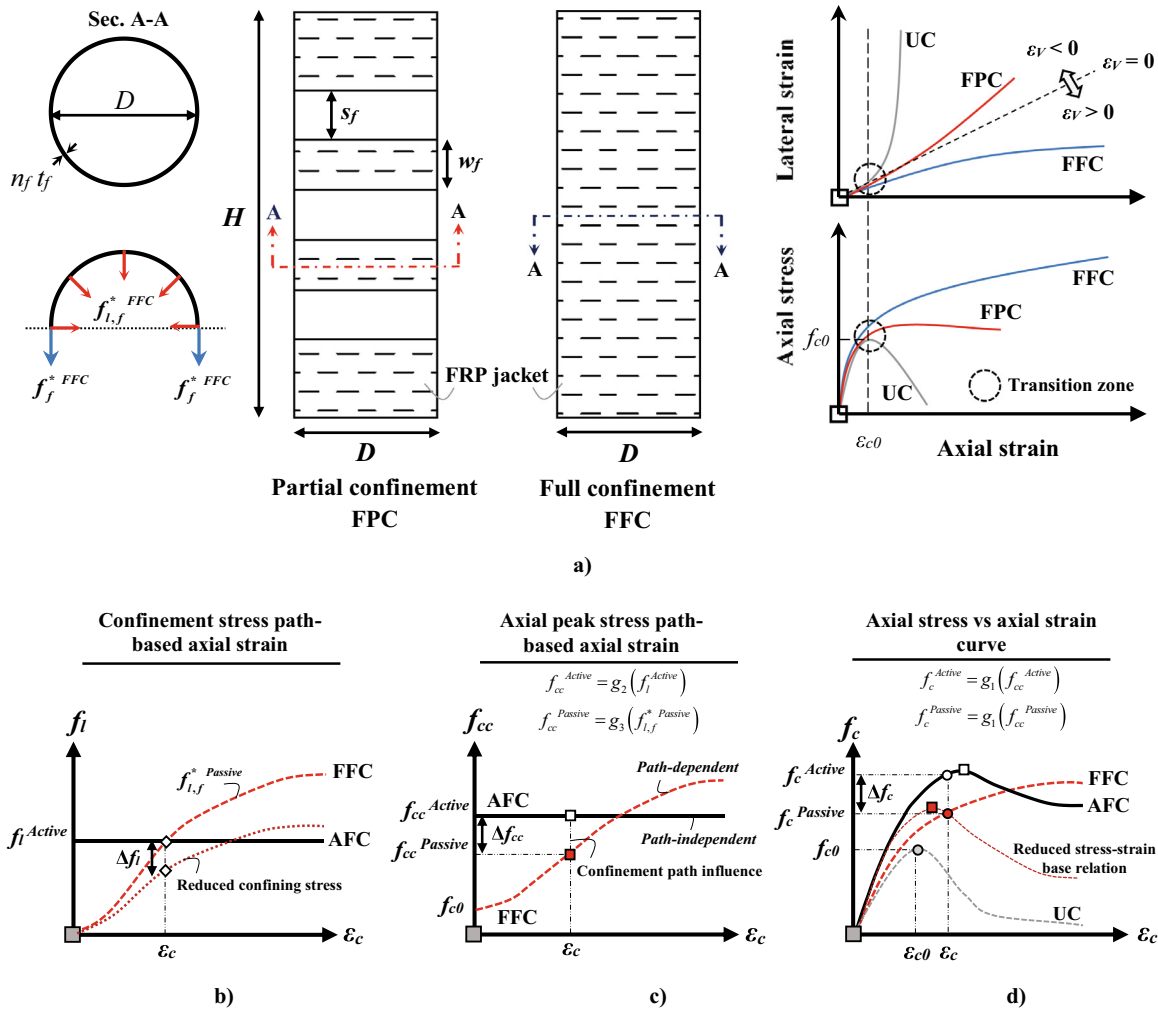


Fig. 1. a) Different confinement configurations; b) Confinement pressure paths of AFC and FFC; c) Peak axial stress vs axial strain; d) Different axial responses of AFC and FFC.

Table 1
Summary of confinement models for AFC and FFC.

Model	Expression		Note
	Axial stress	Peak axial stress	
Category I	$f_c^{Active} = g_1(f_{cc}^{Active})$	$\frac{f_{cc}^{Active}}{f_{c0}} = 1 + m_{a1} \left(\frac{f_{l1}^{Active}}{f_{c0}} \right)^{m_{a2}}$	- $f_c^{Active} = g_2(f_{l1}^{Active})$ - Confinement path-independent- m_{a1} and m_{a2} = calibration factors derived from AFC specimens
Category II	$f_c^{Passive} = g_1(f_{cc}^{Passive})$	$\frac{f_{cc}^{Passive}}{f_{c0}} = 1 + m_{a1} \left(\frac{f_{l1}^{Passive}}{f_{c0}} \right)^{m_{a2}}$	- $f_c^{Passive} = g_2(f_{l1}^{Passive})$ - Confinement path-independent- m_{a1} and m_{a2} = calibration factors derived from AFC specimens
Category III	$f_c^{Passive} = g_1(f_{cc}^{Passive})$	$\frac{f_{cc}^{Passive}}{f_{c0}} = 1 + m_{a1} \left(\frac{f_{l1}^{Passive} - \Delta f_l}{f_{c0}} \right)^{m_{a2}}$ $\frac{f_{cc}^{Passive}}{f_{c0}} = 1 + m_{p1} \left(\frac{f_{l1}^{Passive}}{f_{c0}} \right)^{m_{p2}}$	- $f_c^{Passive} = g_2(f_{l1}^{Passive}, \Delta f_l)$ - Confinement path-dependent- m_{a1} and m_{a2} = calibration factors derived from AFC specimens - $f_c^{Passive} = g_3(f_{l1}^{Passive})$ - Confinement path-dependent- m_{p1} and m_{p2} = the calibration factors derived from FFC specimens

in which f_c^{Active} is the axial stress of AFC as a function of peak axial stress (f_{cc}^{Active}); $f_c^{Passive}$ is the axial stress of FFC as a function of peak axial stress ($f_{cc}^{Passive}$) in the stress-strain base relation; f_{c0} is the axial compressive strength of unconfined concrete; Δf_l is the confinement pressure gradient; Confinement path represents the variation of confinement pressure with axial strain/stress.

ing an axial stress-strain relation (i.e. Popovics [16] suggested for AFC), expressed as a main function of peak axial stress (f_{cc}^{Active}), leading to $f_c^{Active} = g_1(f_{cc}^{Active})$, henceforth designated by stress-strain base relation. In this case, as the most widely adopted framework to date, f_c^{Active} is generally determined as $f_{cc}^{Active} = g_2(f_{l1}^{Active})$ depending on f_{l1}^{Active}

as demonstrated in Table 1. Several studies have been carried out to suggest the calibration factors of m_{a1} and m_{a2} for the g_2 function (Table 1) through using a regression analysis-based method on a set of test database of AFC, which presents the effectiveness of confinement strategy in axial strength enhancements. In Category II (i.e.

[12–14]), conventionally, by adopting a stress–strain base relation, for the case of FFC under a FRP confinement pressure ($f_{lf}^{* Passive}$) assumed to be homogeneously imposed to the entire column height with a variable value during axial loading (Fig. 1b and 1c), its axial stress ($f_c^{Passive}$) at a certain ε_c is considered to be identical to f_c^{Active} through taking into account $f_l^{Active} = f_{lf}^{* Passive}$ ($f_c^{Passive} = g_1(f_{cc}^{Passive})$). However, studies conducted by Lim and Ozbakkaloglu [3], Lin et al. [17] and Yang and Feng [18] demonstrated that this approach, whose development is based on the calibration of m_{a1} and m_{a2} for AFC (Table 1), would lead to overestimations in predicting global axial stress–strain relation of FFC (Δf_c), even though $f_{lf}^{Active} = f_{lf}^{Passive}$ at a certain ε_c , as highlighted in Fig. 1b-d. It can be attributed to the considerable difference in the confinement pressure path imposed to concrete in AFC and FFC with constant and variable trends, respectively, as presented in Fig. 1b. Confinement pressure path in the present context represents the relation between confinement pressure and axial stress/strain during the entire axial compressive loading. Category III includes analysis-oriented models formulating the noticeable influence of confinement pressure path on axial response of FFC. In this category, Lim and Ozbakkaloglu [3] introduced the concept of a reduced stress–strain base relation for the case of FFC to reflect this effect in the calculation of $f_{cc}^{Passive}$ through applying a reduction Δf_l in the actual FRP confinement pressure obtained from dilation model. In this model, as presented in Fig. 1b, Δf_l represents the gradient of confinement pressure that was suggested empirically as a function of confinement stiffness (known as the ratio of FRP confinement pressure over concrete lateral strain), concrete compressive strength and the corresponding concrete lateral strain. Yang and Feng [18] proposed a refined version of Jiang and Teng [12]’s model (Category II) to account for the difference in confinement pressure paths of FFC and AFC in terms of the peak axial stress of the stress–strain base relation (Δf_{cc}). In this approach, the calibration factors of m_{p1} and m_{p2} (Table 1) were derived from a set of test results of FFC specimens. It was also demonstrated that this effect plays a key role in the establishment of global axial stress–strain response of FCC. Based on Zhao et al. [19]’s model originally suggested for concrete-filled steel tube columns, Lin et al. [17] investigated the influence of confinement pressure path on ultimate axial stress of FFC, which was demonstrated to be a function of the level of confinement pressure at FRP rupture and concrete compressive strength. By considering this effect in the establishment of ultimate axial stress of FFC, the model demonstrated a better performance in predicting the experimental counterparts. Nonetheless, to the best of the authors’ knowledge, the substantial influence of confinement pressure path on axial stress–strain response of FFC has not been investigated comprehensively in the existing models. Accordingly, the development of a confinement model addressing confinement pressure path to predict the global axial stress–strain of FFC with a unified approach with FFC is still lacking.

On the other hand, in existing analysis-oriented models, in general, for the sake of the simplicity, by assuming a uniform distribution of concrete expansion for FFC, confinement pressure ($f_{lf}^{* Passive}$) is subsequently considered to be homogenous along the column height. However, this assumption is only acceptable prior to the loading stage corresponding to the peak axial stress of unconfined concrete. Beyond this stage, the rate of concrete lateral expansion tends to significantly increase due to the development of longitudinal concrete cracking, leading to a non-uniform distribution of concrete transversal dilatancy, particularly in the case of FRP lightly confined concrete [20–22]. Wu and Wei [20] performed axial compressive tests on FFC, FPC and unconfined concrete (UC) columns to examine the distribution of concrete lateral strain along the column height. It was highlighted that during axial loading, concrete would experience a non-uniform distribution of expansion depending on confinement configuration. To

evaluate the influence of confinement on concrete axial/lateral strain distribution of FFC along the column height, Fallahpour et al. [22] conducted an experimental investigation through Digital Image Correlation (DIC) technique for the measurement of full-field strain evolution. The test results demonstrated that FFC only with high confinement stiffness revealed relatively homogenous axial and dilation responses, while in the case of lower confinement stiffness, less uniform behavior along with local strain gradients was exhibited. Therefore, since the generation of FRP confining hoop strain/stress is in a direct relation with concrete dilation behavior, the generated confining stress would be imposed non-homogeneously on the concrete as a main function of confinement stiffness. As a result, the assumption of uniform confinement pressure ($f_{lf}^{* Passive}$) can be considered to be acceptable only for highly-confined concrete. For the case of low confinement stiffness with non-homogenous confining stress distribution, this assumption does not seem to adequately comply the described experimental observations. For the case of FPC, Zeng et al. [7] experimentally evidenced the distribution of concrete expansion would be predominantly non-homogenous, particularly in case of large s_f (distance between strips of FRP, Fig. 1a), as also confirmed by Guo et al. [8,9]. Shayanfar et al. [23] presented a refined version of the concept of confinement efficiency factor, originally suggested by Mander et al. [24] for concrete confined partially with steel stirrups, by formulating the non-homogenous distribution of concrete dilatancy of FPC, besides the influence of vertical arching action. However, in this model, the pattern of concrete expansion of FFC was assumed as uniform, for the sake of simplicity. Therefore, to the best of the authors’ knowledge, the influence of non-homogenous distribution of concrete expansion along the column height of FFC/FPC on the determination of confinement pressure and subsequently, axial and dilation responses has not been addressed comprehensively in the existing analysis/design-oriented models.

The present study is dedicated to the development of a generalized confinement model, applicable to full and partial confinement arrangements applied on circular cross section concrete columns, by using a unified approach in the prediction of their axial and dilation responses. For formulating the influence of concrete expansion distribution in the calculation of confinement pressure, Shayanfar et al. [23]’s model is extended to be applicable to FFC as a function of confinement stiffness, along with some refinements for the case of FPC. A new analysis-oriented model as confinement-path dependent in compliance with Category III is proposed for the establishment of the axial stress–strain curve of FFC and FPC, by introducing new calibration factors of m_{p1} and m_{p2} depending on confinement stiffness. A new expression is subsequently developed to estimate ultimate axial strain of FFC/FPC by combining theoretical knowledge and experimental observations. Finally, the reliability of the developed model is vastly examined by simulating the global axial stress–strain curves registered experimentally in available literature. The comparative assessment of the predicted performance in term of ultimate axial stress/strain obtained from the developed model versus by *fib* [25], CNR DT 200/2004 [26] and ACI 440.2R-17 [27] approaches (briefly presented in Appendix A) is also demonstrated.

2. Proposed confinement model for FFC

This section provides the determination of the confinement characteristics of FFC under axial compressive loading. The effectiveness of FRP confining system to limit concrete dilatancy during axial loading is dependent on the level of confinement pressure. For the case of full confinement with a uniform concrete expansibility along the column height (assuming identical hoop and radial strain $\varepsilon_h = \varepsilon_{lj}$), the FRP confining stress, $f_f^{* FFC}$, and the FRP confinement pressure, $f_{lf}^{* FFC}$, can be derived using force equilibrium conditions (Fig. 1a):

$$f_{l_j}^{*FFC} = 2 \frac{n_f t_f}{D} f_j^{*FFC} = 2 \frac{n_f t_f}{D} E_f \epsilon_{l_j} \quad (1)$$

where n_f is the number of FRP layers, t_f is the FRP thickness, D is the diameter of the column, E_f is the FRP modulus elasticity, and ϵ_{l_j} is the maximum concrete lateral expansibility along with the assumption of perfect bond between FRP and concrete substrate. Nevertheless, the studies conducted by Wu and Wei [20] and Wei and Wu [21] demonstrated that the distribution of the concrete lateral expansion in the case of FFC system during axial compressive loading would vary along the column height as a function of confinement stiffness. As shown in Fig. 2, the maximum (ϵ_{l_j}) and minimum (ϵ_{l_i}) concrete lateral expansibility can be assumed to occur at the Point j and Point i , respectively, with the distance of L_d defining the damage zone length, which will be addressed in detail in Section 3. Consequently, at a certain level of ϵ_{l_j} , the maximum and minimum FRP confining stresses are $f_{f_j}^{FFC} = E_f \epsilon_{l_j}$ and $f_{f_i}^{FFC} = E_f \epsilon_{l_i}$, respectively. In this study, the reduction factor k_{ff} is introduced to determine an average FRP confining stress

(f_f^{FFC}) uniformly applied on the columns in order to account for the non-uniform concrete expansibility:

$$f_f^{FFC} = k_{ff}^{FFC} f_{f_j}^{FFC} = k_{ff}^{FFC} E_f \epsilon_{l_j} \quad (2)$$

Based on Eq. (1), FRP confinement pressure ($f_{l_j}^{FFC}$) resulting from f_f^{FFC} can be expressed as:

$$f_{l_j}^{FFC} = 2 \frac{n_f t_f}{D} f_f^{FFC} = 2 \frac{n_f t_f}{D} k_{ff}^{FFC} E_f \epsilon_{l_j} \quad (3)$$

For the sake of simplicity, the reduction factor k_{ff} , can be determined by taking an average of the $\epsilon_{l(z)}/\epsilon_{l_j}$ ratio along the damage zone (Fig. 3):

$$k_{ff}^{FFC} = 2 \frac{\int_0^{L_d/2} \frac{\epsilon_{l(z)}}{\epsilon_{l_j}} dz}{L_d} = 2 \frac{\int_0^{L_d/2} k_\epsilon(z) dz}{L_d} \quad (4)$$

where $\epsilon_{l(z)}$ defines the concrete lateral strain within the damage zone (L_d) along the z axis as illustrated in Fig. 3. Considering a second order

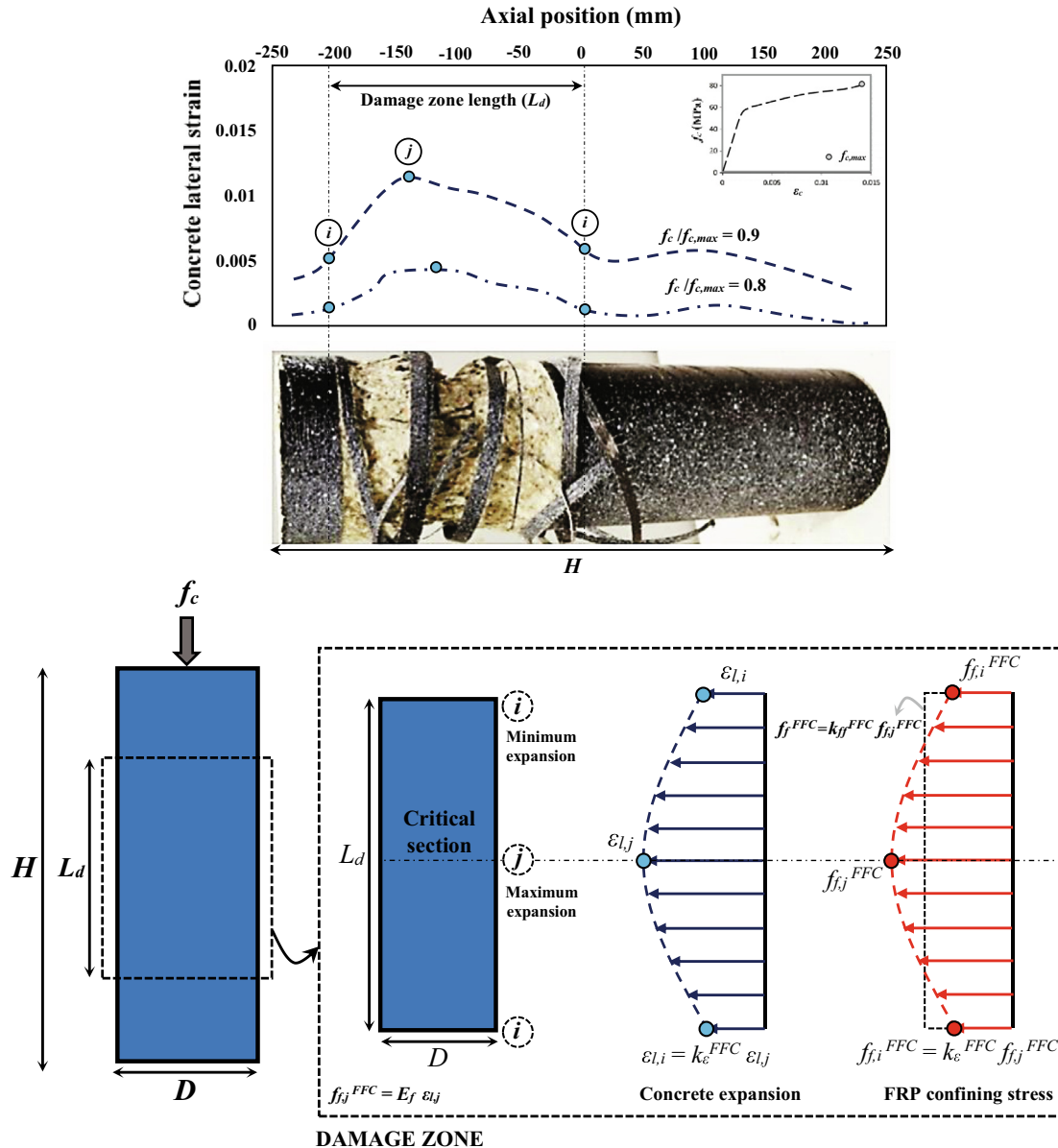


Fig. 2. Distribution of concrete lateral expansion and FRP confining stress.

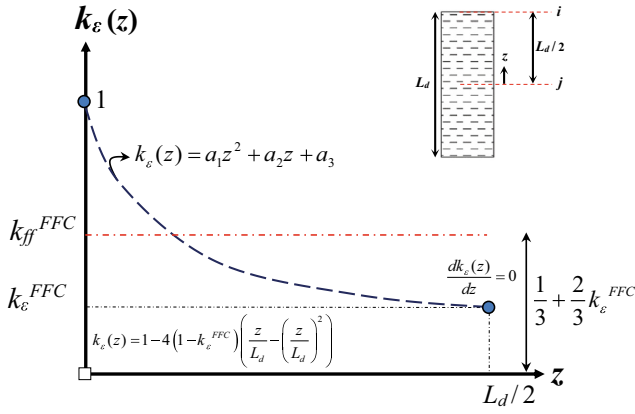


Fig. 3. Distribution $k_e(z)$ along $L_d/2$.

parabola function distribution for $k_e(z)$ along with $k_e = k_e^{FFC}$ and $dk_e(z)/dz = 0$ at the point i ($z = L_d/2$), leads to (Fig. 3):

$$k_{ff}^{FFC} = \frac{2 \int_0^{L_d/2} (a_1 z^2 + a_2 z + a_3) dz}{L_d}$$

$$= \frac{2 \int_0^{L_d/2} \left[1 - 4(1 - k_e^{FFC}) \left(\frac{z}{L_d} - \left(\frac{z}{L_d} \right)^2 \right) \right] dz}{L_d} = \frac{1}{3} + \frac{2}{3} k_e^{FFC} \quad (5)$$

where k_e^{FFC} is the ratio between ε_{li} and ε_{lj} . For highly-confined concrete by FRP confinement pressure, concrete transversal expansibility tends to be uniform, leading to $k_e^{FFC} = 1$ and according to Eq. (5), $k_{ff}^{FFC} = 1$. In this case, the volumetric strain would be positive during axial compressive loading ($\varepsilon_V \geq 0$), as shown in Fig. 4, representing a specimen's volume decrease. On the other hand, lightly-confined concrete experiences a noticeable variation in expansion, depending on the confinement stiffness. In this study, based on Teng et al. [28] achievements, for FFC with uniform concrete expansibility, confinement stiffness index I_f can be determined as:

$$I_f = \frac{f_{lf}^{FFC} / (k_{ff}^{FFC} \varepsilon_{lj})}{f_{c0} / \varepsilon_{c0}} = 2 \frac{n_f t_f E_f \varepsilon_{c0}}{D f_{c0}} \quad (6)$$

in which

$\varepsilon_{c0} = 0.0015 + \frac{f_{c0}}{70000}$ (f_{c0} in MPa) (7) where ε_{c0} is the axial strain corresponding to f_{c0} , as suggested by Karthik and Mander [29]. Fig. 4

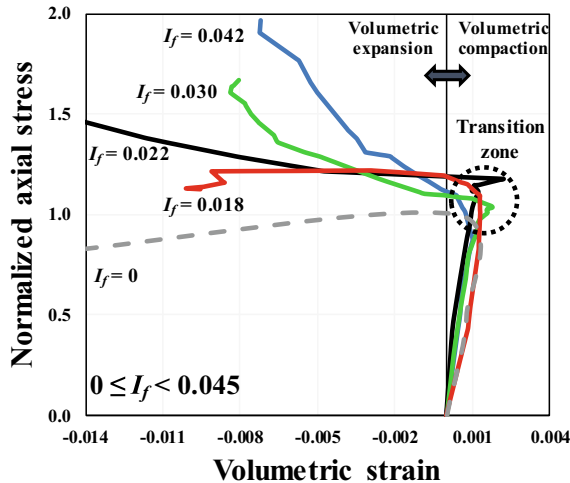


Fig. 4. Normalized axial stress vs volumetric strain.

shows the relation between the normalized axial stress (f_c/f_{c0}) and volumetric strain ($\varepsilon_V = \varepsilon_c - 2\varepsilon_{lj}$) for the test specimens conducted by Wang and Wu [30], Eid et al. [31], Lim and Ozbakkaloglu [4] and Zeng et al. [5] with different I_f . As can be seen, the confinement configurations corresponding to the confinement stiffness index less than 0.045 are not capable of controlling concrete dilation, with concrete dilation as high as smaller is I_f . Teng et al. [28] recommended that for lightly confined concrete ($I_f \leq 0.01$), the effectiveness of confinement pressure on axial and dilation response can be neglected. At I_f of about 0.045, the volumetric strain evolution virtually becomes reversed due to FRP jacket capability to restrain the concrete expansion. For $I_f \geq 0.045$, since the FRP confinement pressure is significantly activated, the confined concrete drives to behave in a compaction way. Accordingly, for high value of I_f with $\varepsilon_V \geq 0$, the distribution of concrete expansion of FFC is expected to be approximately uniform with $k_e^{FFC} = \varepsilon_{li}/\varepsilon_{lj} \approx 1$. To evaluate the influence of confinement on concrete axial/lateral strain distribution of FFC along the column height, Fallahpour et al. [22] experimentally evidenced that FFC only with high confinement stiffness ($I_f = 0.061$) revealed relatively homogenous axial and dilation responses, while in the case of lower confinement stiffness, less uniform behavior along with local strain gradients (leading to a low value of k_e^{FFC}) was exhibited.

Based on the aforementioned discussion, using the dilation model developed by Shayanfar et al. [23] (Eq. (8)), when $\varepsilon_V = 0$, the value of confinement stiffness index (I_f^*) corresponding to the maximum secant Poisson's ratio ($\nu_{s,max}$) equal to 0.5 can be determined by Eq. (9).

$$\nu_{s,max} = \frac{0.155}{(1.23 - 0.003f_{c0})\sqrt{I_f}} \quad (8)$$

$$I_f^* = \left(\frac{0.155}{(1.23 - 0.003f_{c0}) \times 0.5} \right)^2 \approx 0.06 + 0.0005f_{c0} \quad (f_{c0} \text{ in MPa}) \quad (9)$$

Accordingly, based on the experimental observations conducted by Fallahpour et al. [22] for $I_f < I_f^*$, a non-uniform distribution of concrete expansion with maximum and minimum lateral strains at Point j and Point i , respectively, can be assumed, so that $k_e^{FFC} < 1$. Based on the above discussion, to develop the relation between k_e^{FFC} and I_f , the following conditions should be satisfied:

- i. k_e^{FFC} enhances with increasing I_f .
- ii. k_e^{FFC} approaches the value of $k_{e,min}$ when confinement pressure is equal to zero (unconfined concrete).

iii. k_e^{FFC} approaches 1 when $I_f \geq I_f^*$ as evidenced by Fallahpour et al. [22].

Shayanfar et al. [23,32] recommended $k_{e,min} = 0.08$ based on the experimental dilation results of a series of unconfined concrete specimens. Considering the aforementioned conditions, a new expression was derived to determine k_e^{FFC} from I_f and I_f^* (Fig. 5):

$$k_e^{FFC} = 0.08 + 0.92 \left[2 \frac{I_f}{I_f^*} - \left(\frac{I_f}{I_f^*} \right)^2 \right] \leq 1 \text{ for } I_f \leq I_f^* \quad (10)$$

$$k_e^{FFC} = 1 \quad \text{for } I_f \geq I_f^* \quad (10)$$

Ultimately, by determining k_e^{FFC} depending on I_f , k_{ff}^{FFC} can be obtained using Eq. (5) as an input parameter in Eq. (3) for the calculation of f_{lf}^{FFC} .

3. Proposed confinement model for FPC

This section is dedicated to address the determination of the confinement characteristics of partially confined concrete (FPC) columns under axial compressive loading. In Fig. 6, the non-uniform distributions of concrete lateral expansion and FRP partial confining stress in FPC are presented. As can be seen, the maximum expansion ϵ_{lj} would occur at the critical section corresponding to Point j , which is not directly subjected to confinement pressure. However, point i corresponding to middle section of FRP strip experiences the minimum concrete dilatancy, ϵ_{li} , leading to FRP confining stress $f_{f,i}$. In this study, according to Eqs. (1) to (3), considering the influence of vertical arching action based on Shayanfar et al. [32] presented in Eq. (14), FRP confinement pressure (f_{lf}^{FFC}) generated by f_{ff}^{FFC} can be expressed as:

$$f_{lf}^{FFC} = 2 \frac{n_f t_f w_f}{(s_f + w_f) D} k_p k_{v,f} f_{ff}^{FFC} = 2 \frac{n_f t_f}{D} k_p k_{v,f} f_{ff}^{FFC} \quad (11)$$

in which

$$f_{ff}^{FFC} = k_{ff}^{FFC} f_{fj}^{FFC} = k_{ff}^{FFC} E_f \epsilon_{lj} \quad (12)$$

$$k_p = \frac{w_f}{s_f + w_f} \quad (13)$$

$$k_{v,f} = \frac{w_f + s_f (1 - R_f + 0.43R_f^2 - 0.07R_f^3)}{w_f + s_f} \leq 1 \quad (14)$$

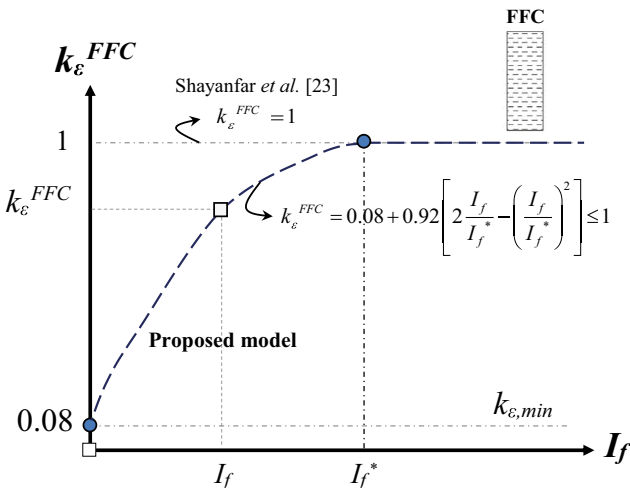


Fig. 5. k_e^{FFC} versus I_f relation.

$$R_f = \frac{s_f}{D} \quad (15)$$

where w_f is the strip width. R_f is a non-dimensional parameter. It should be noted that, due to vertical arching action mechanism between two consecutive strips, confinement pressure effectiveness on this zone can be very distinct from the one corresponding to full confinement. Based on the concept of the confinement efficiency factor ([24]), by applying the reduction factor $k_{v,f}$, the entire concrete column can be assumed to be as effectively confined concrete, similar to FFC confinement mechanism.

According to the developed relation for FFC ($s_f = 0$), by increasing s_f in FPC system, the confinement system capability to curtail concrete transversal expansibility decreases. Accordingly, for a relatively large value of s_f , the effectiveness of this partial confining system becomes minimal and approaches to $k_{e,min} = 0.08$, while k_{ff}^{FFC} can be assumed as k_{ff}^{FFC} when $s_f = 0$. In this study, for $s_f \geq L_d$, representing the condition that the damage zone occurs between FRP strips, the effect of confinement was conservatively ignored and its dilation behavior would be similar to that of unconfined concrete (Wei and Wu [21]). Consequently, for this case, L_d can be estimated to be equal to the length of damage zone of unconfined concrete columns (L_{d0}). By using the concept of localized compressive fracture length proposed by Lertsrisakurat et al. [33], Wu and Wei [20] recommended an empirical equation to calculate L_{d0} as a function of column diameter and concrete compressive strength as follows (with a slight rearrangement):

$$0.57 \leq \frac{L_{d0}}{D_{Ler} \psi_f} = 1.71 - 3.53 \times 10^{-5} D_{Ler}^2 \leq 1.36 \quad (16)$$

in which

$$D_{Ler} = \sqrt{A_g} \approx 0.886D \quad (D \text{ in MPa}) \quad (17)$$

$$\psi_f = \frac{6.3}{\sqrt{f_{c0}}} \leq 1 \quad (f_{c0} \text{ in MPa}) \quad (18)$$

where D_{Ler} is the equivalent diameter that is calculated as the square root of the total cross-sectional area [33].

To develop the relation between k_{ff}^{FFC} and s_f , the following conditions should be satisfied:

- i. k_{ff}^{FFC} decreases with the increase of s_f .
- ii. k_{ff}^{FFC} is equal to k_e^{FFC} when $s_f \approx L_{d0}$
- iii. k_{ff}^{FFC} follows a hoop strain distribution similar to FFC when $s_f \approx 0$
- iv. k_{ff}^{FFC} approaches the value of $k_{e,min}$ when $s_f \approx L_{d0}$ (unconfined concrete).
- v. k_{ff}^{FFC} approaches k_{ff}^{FFC} when $s_f \approx 0$.

Therefore, the relation between k_{ff}^{FFC} and s_f/L_{d0} was formulated to decrease linearly from $k_{ff}^{FFC} = k_{ff,ave}^{FFC}$ at $s_f = 0$ (full confinement) to $k_{ff}^{FFC} = 0.08$ at $s_f = L_{d0}$:

$$k_{ff}^{FFC} = k_{ff,ave}^{FFC} - \left(k_{ff,ave}^{FFC} - k_e^{FFC} \right) \frac{s_f}{L_{d0}} \geq 0.08 \quad (19)$$

in which

$$k_{ff,ave}^{FFC} = \frac{1}{3} + \frac{2}{3} k_e^{FFC} \quad (20)$$

where $k_{ff,ave}^{FFC}$ represents the ratio of average hoop strain and maximum hoop strain within the damage zone, based Eq. (5) with a uniform approach with FFC, when the distribution of concrete lateral strain would be identical to full confinement in the case of $s_f = 0$. Introducing Eq. (20) into Eq. (19) gives

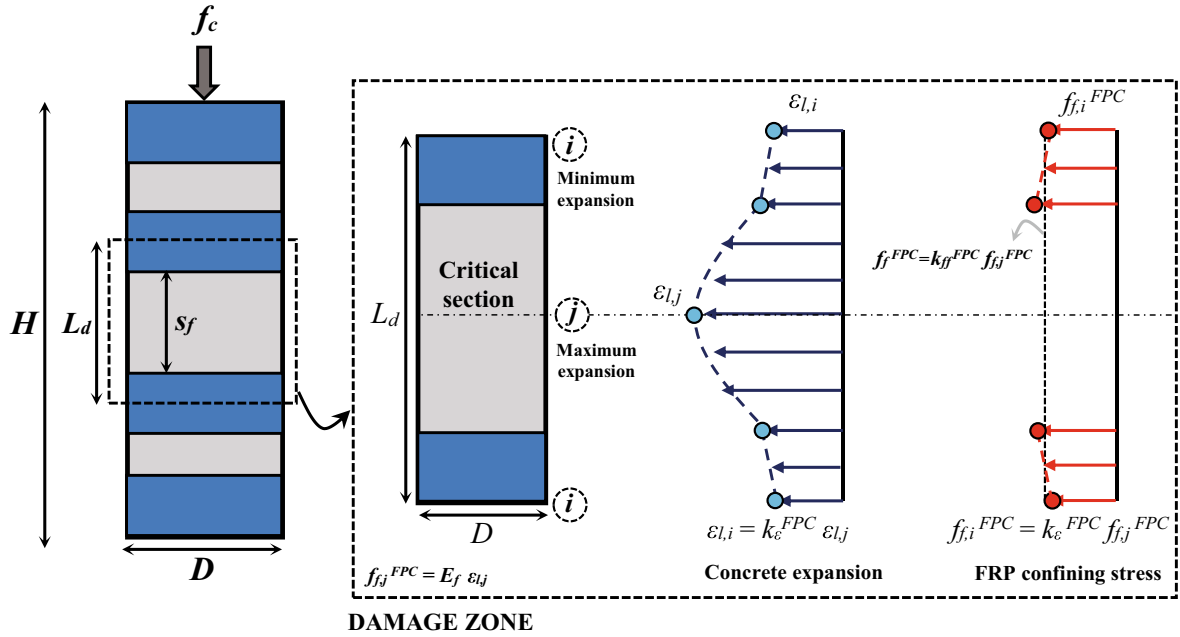


Fig. 6. Distributions of concrete lateral expansion and FRP confining stress for FPC.

$$k_{ff}^{FPC} = \frac{1}{3}(1 + 2k_e^{FPC}) - \frac{s_f}{3L_{d0}}(1 - k_e^{FPC}) \geq 0.08 \quad (21)$$

For the determination of k_e^{FPC} , based on Eq. (19), it was assumed that it linearly decreases from $k_e^{FPC} = k_e^{FPC}$ (at $s_f/L_{d0} = 0$, full confinement) to $k_e^{FPC} = 0.08$ (at $s_f = L_{d0}$) (Fig. 7):

$$k_e^{FPC} = k_e^{FPC} - (k_e^{FPC} - 0.08) \frac{s_f}{L_{d0}} \geq 0.08 \quad (22)$$

Accordingly, by replacing k_e^{FPC} obtained from Eq. (22) in Eq. (21), k_{ff}^{FPC} can be determined, as an input parameter in Eq. (12). The k_{ff}^{FPC} versus s_f/L_{d0} relationship for FPC is demonstrated in Fig. 7. It estimates k_{ff}^{FPC} lower than Shayanfar et al. [23] model due to the consideration of a non-uniform distribution for concrete lateral expansion in case of FFC.

It is now well-established that the FRP confinement-induced improvements in FFC and FPC substantially depend on the confinement stiffness imposed on the confined concrete. For reflecting the influence of this parameter, the recommendation of Shayanfar et al.

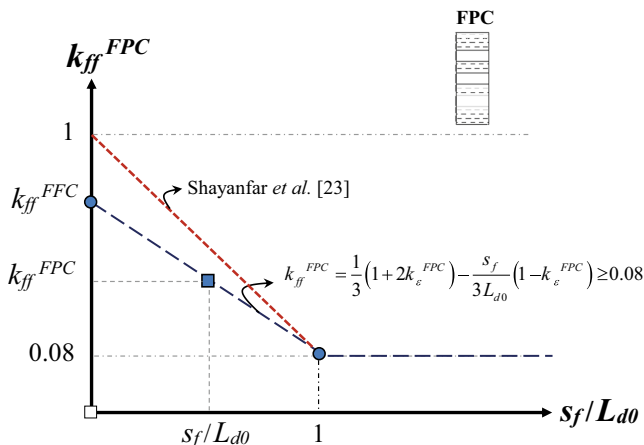


Fig. 7. k_{ff}^{FPC} versus s_f/L_{d0} relation.

[23] was taken, by proposing a new confinement stiffness index applicable to both full and partial systems, taking into account the concrete transversal expansibility (by considering Eqs. (6), (11) and (12)):

$$\rho_{Kf} = \frac{f_{lf}^{FPC}/\epsilon_{lj}}{f_{c0}/\epsilon_{c0}} = k_p k_{v,f} k_{ff}^{FPC} I_f = K_e I_f \quad (23)$$

in which

$$K_e = k_p k_{v,f} k_{ff}^{FPC} \quad (24)$$

where K_e is defined as the confinement efficiency factor. For FFC, Eq. (23) leads to $\rho_{Kf} = k_{ff}^{FPC} I_f$ that can be calculated using Eqs. (5) and (6), respectively.

4. Dilation model

This section is dedicated to address the determination of the dilation characteristics for FFC and FPC. According to the confinement mechanism, at a certain axial stress, f_c , the corresponding ϵ_c leads to lateral strain ϵ_{lj} (radial strain) in compliance with concrete secant Poisson's ratio ν_s , resulting in confining stress to restrain concrete tendency to dilate. By rearranging Eq. (23), FRP confinement pressure can become explicitly dependent on ν_s :

$$\frac{f_{lf}^{FPC}}{f_{c0}} = \rho_{Kf} \frac{\epsilon_{lj}}{\epsilon_{c0}} = \rho_{Kf} \frac{\nu_s \epsilon_c}{\epsilon_{c0}} \quad (25)$$

Accordingly, the determination of ν_s corresponding to ϵ_c is essential for calculating the confinement pressure. Based on a large database of the experimental dilation responses of FFC and FPC, Shayanfar et al. [23] proposed a strategy to calculate the relation between $\nu_s/\nu_{s,max}$ and ϵ_c , as illustrated in Fig. 8. Here, $\nu_s/\nu_{s,max}$ is the secant Poisson's ratio normalized by its maximum value at the critical section during axial loading corresponding to the axial strain of $\epsilon_{c,m}$, which was empirically suggested as:

$$\epsilon_{c,m} = 0.0085 - 0.05\rho_{Kf} \quad (26)$$

As shown in Fig. 8, the dilatancy of confined concrete is equal to that of unconfined concrete up to $\epsilon_c = \epsilon_{c0}$ (point A) with $\nu_s = \nu_{s,0}$, which can be calculated by (Candappa et al. [34]):

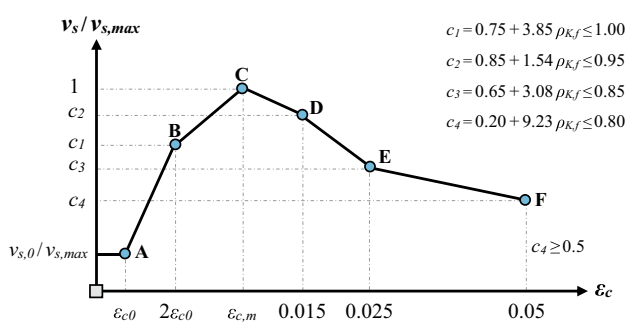


Fig. 8. $v_s/v_{s,max}$ and ϵ_c relation (redrawn from Shayanfar et al. [23]).

$$v_{s,0} = 8 \times 10^{-6} f_{c0}^2 + 2 \times 10^{-4} f_{c0} + 0.138 \quad (f_{c0} \text{ in MPa}) \quad (27)$$

Since the development of concrete cracking induces an increase in v_s , the trend evolves from $v_{s,0}$ to $C_1 \times v_{s,max}$ (point B), corresponding to $\epsilon_c = 2\epsilon_{c0}$ ([25]), and further increases up to $v_{s,max}$ at $\epsilon_c = \epsilon_{c,m}$ (point C), followed by a decrease until ultimate conditions. To formulate the relation between v_s and ϵ_c , the determination of $v_{s,max}$ as an input parameter is necessary, which was derived empirically through regression analysis method. The test database (Table 2), used for deriving/calibrating the model parameters in the present study, consists of the test specimens of FFC and FPC with a wide range of material properties. It comprises $70 \leq D \leq 300$ (mm), $15.8 \leq f_{c0} \leq 171.0$ (MPa), $13.6 \leq E_f \leq 276.0$ (MPa), $0.013 \leq \epsilon_{fu} \leq 0.035$, $0.001 \leq \rho_{K,f} \leq 0.262$ and different FRP types as carbon, glass, basalt and aramid FRP (CFRP, GFRP, BFRP, AFRP).

Fig. 9a demonstrates the variation of $v_{s,max}$ with $\rho_{K,f}$ based on the test database by Shayanfar et al. [23]. As expected, the $v_{s,max}$ decreases with the increase of the confinement stiffness, as $v_{s,max} = 0.15/\sqrt{\rho_{K,f}}$ using a preliminary regression analysis (Fig. 9a). The decrease is quite abrupt up to $\rho_{K,f} \cong 0.015$, and smooth above this value. In the present study, based on the best fit with experimental results, a new formulation to calculate $v_{s,max}$ as a main function of $\rho_{K,f}$ (along with L_{d0}/D) was developed, resulting in:

$$v_{s,max} = \frac{0.15}{(0.585 + 0.585 \frac{L_{d0}}{D}) \sqrt{\rho_{K,f}}} = \frac{0.256}{(1 + \frac{L_{d0}}{D}) \sqrt{\rho_{K,f}}} \quad (28)$$

The acceptable predictive performance of Eq. (28) in the simulation of the experimental counterparts can be confirmed in Fig. 9b.

5. Model to determine the axial stress–strain response

This section addresses the establishment of the axial stress–strain relation of circular cross section concrete columns with FFC and FPC arrangements. A new model in compliance with Category III is proposed by introducing new calibration factors of m_{p1} and m_{p2} as presented in Table 1. In this category, at a certain level of axial strain (ϵ_c), the corresponding axial stress (f_c) can be determined by adopting a stress–strain base relation, whose characteristics are expressed as a function of the peak stress (f_{cc}) and the corresponding axial strain (ϵ_{cc}).

To formulate f_c versus ϵ_c relation as a stress–strain base relation, the expression suggested by Popovics [16], originally for AFC, was adopted:

$$f_c = f_{cc} \frac{(\epsilon_c/\epsilon_{cc})^n}{n - 1 + (\epsilon_c/\epsilon_{cc})^n} \quad (29)$$

in which

$$\frac{\epsilon_{cc}}{\epsilon_{c0}} = 1 + 5 \left(\frac{f_{cc}}{f_{c0}} - 1 \right) \quad ([25]) \quad (30)$$

$$n = \frac{E_c}{E_c - f_{cc}/\epsilon_{cc}} \quad (31)$$

$$E_c = 4400 \sqrt{f_{c0}} \quad (f_{c0} \text{ in MPa}) \quad (32)$$

where n defines the concrete brittleness introduced by Carreira and Chu [47]; E_c is the modulus elasticity of concrete proposed by Lim and Ozbakkaloglu [15].

In the present study, according to Yang and Feng [18], a new strength model in compliance with Category III (Table 1) is developed to determine the relation between f_{cc} and f_{lf}^{FPC} (which is determined from Eq. (25)), derived from global axial stress–strain of FFC/FPC test specimens with passive confinement path. It can be expressed as

Table 2
Assembled database for FFC and FPC.

ID	Total	Confinement arrangement		D (mm)	f_{c0} (MPa)	$\rho_{K,f}$	R_1	R_2	$\frac{f_{cu}}{f_{c0}}$	$\frac{\epsilon_{cu}}{\epsilon_{c0}}$
		FFC	FPC							
Rochette and Labossie're [35]	2	2		100–150	44–45	2.6–4.2	1.97–2.35	0.75–0.86	1.6–1.7	7.2–7.7
Shehata et al. [36]	2	2		150	26–30	3.2–6.6	3.15–3.72	0.76–0.91	2.1–2.4	7.8–9.3
Teng and Lam [37]	3	3		152	37–39	1.5–3.9	3.15–3.82	0.64–0.80	1.4–1.9	4.5–8.2
Xiao and Wu [38]	39	39		152	34–55	1.3–8.5	0.62–3.81	0.68–1.05	1.0–2.8	1.9–12.7
Berthet et al. [39]	15	15		70–160	23.6–171	1.3–15.1	1.10–4.5	0.62–1.01	1.1–2.2	1.6–8.7
Barros and Ferreira [6]	39	8	31	150	18–40	0.1–26.2	0.18–4.86	0.34–1.40	1.0–6.5	2.9–28.1
Wang and Wu [30]	4	4		150	31–52	1.3–5.9	1.00–2.98	0.67–0.90	1.3–2.2	4.8–14.3
Eid et al. [31]	18	18		152	32–68	1.1–6.9	0.71–3.47	0.59–0.93	1.2–2.2	2.7–11.1
Wang and Wu [40]	18	18		70–194	24–52	0.3–5.1	0.19–2.85	0.37–0.89	1.0–3.4	1.5–6.0
Benzaid and Mesbah [41]	6	6		160	26–62	1.0–9.2	0.72–4.10	0.63–0.95	1.1–2.5	1.5–11.9
Lim and Ozbakkaloglu [4]	36	36		152	30–98	0.9–5.2	1.02–3.46	0.59–0.91	1.2–2.0	5.5–12.1
Vincent and Ozbakkaloglu [42]	6	6		152	110	2.7–4.8	1.16–1.73	0.80–0.90	1.2–1.5	5.4–6.9
Zeng et al. [43]	12	3	9	238	23	0.9–8.9	0.45–4.16	0.39–0.95	1.3–3.1	2.7–10.9
Zeng et al. [5]	60	6	54	150	23	0.1–13.0	0.20–4.25	0.31–1.16	1.1–4.7	5.2–26.8
Zeng et al. [7]	15	15		150	24	0.1–4.1	0.19–2.07	0.33–0.81	1.0–1.8	4.1–17.3
Wang et al. [44]	7	1	6	100	36	0.1–5.7	0.17–4.35	0.35–0.88	1.2–4.0	1.5–18.6
Guo et al. [8]	21		21	100–300	34–42	0.2–3.8	0.28–2.61	0.47–0.68	1.1–2.2	6.3–25.0
Suon et al. [45]	3	3		150	16	0.9–3.8	1.10–3.25	0.55–0.77	1.5–2.4	6.4–12.8
Shan et al. [46]	3	3		300	37	3.8	3.42	0.79	2.1–2.2	6.5–6.6
Lin et al. [17]	18	18		150	32–54	3.2–14.5	3.11–4.31	0.75–1.23	1.3–3.7	5.4–19.1
ALL	327	191	136	155 ^a -0.22 ^b	40–0.56	3.6–0.94	1.79–0.65	0.68–0.37	1.8–0.38	9.3–5.9

Note: a: Mean; b: CoV.

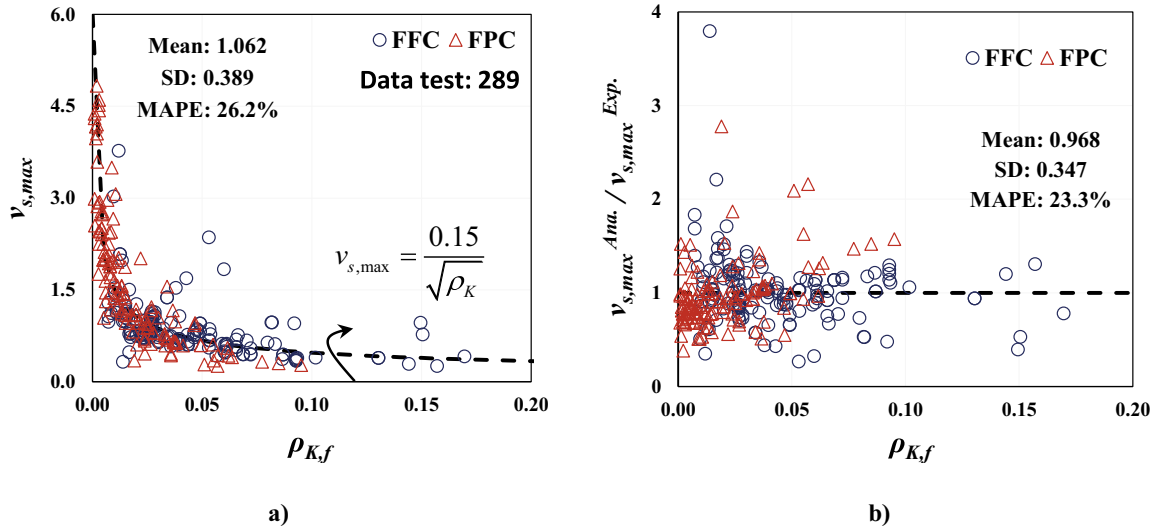


Fig. 9. a) Variation of the experimental dilation results with $\rho_{K,f}$; b) Predictive performance of Eq. (28).

$$\begin{aligned} \frac{f_{cc}}{f_{c0}} &= 1 + m_{p1} \left(\frac{f_{lf}^{Passive}}{f_{c0}} \right)^{m_{p2}} = 1 + \frac{R_1}{R_2} \left(\frac{f_{lf}^{FPC}}{f_{c0}} \right)^{R_2} \\ &= 1 + \frac{R_1}{R_2} \left(\rho_{K,f} \frac{v_s \epsilon_c}{\epsilon_{c0}} \right)^{R_2} \end{aligned} \quad (33)$$

where R_1 and R_2 are the terms introduced to calibrate this equation. For this purpose, the extracted experimental R_1 and R_2 were determined using back analysis method performed on the global axial stress–strain of FFC/FPC test specimens. It is because that contrary to the case of AFC in which f_{cc}^{Active} as a function of f_l^{Active} is constant during entire axial loading, f_{cc} significantly varies with f_{lf}^{FPC} in the case of passive confinement. Accordingly, calibrating Eq. (33) just based on the failure stage of the test specimens does not sufficiently reflect the relation of f_{cc} and f_{lf}^{FPC} . Therefore, in the present study, considering the variable relation of f_{cc} and f_{lf}^{FPC} depending on the level of axial strain, based on the best fitting with the experimental f_c vs ϵ_c curves collected in the test database, these parameters as a main function of the developed confinement stiffness index ($\rho_{K,f}$) were determined as;

$$R_1 = \frac{23.9 \rho_{K,f}^{0.67}}{\lambda_{fc} \lambda_{Rf} \lambda_D} \leq 4.25 \quad (34)$$

$$R_2 = 1.85 \rho_{K,f}^{0.26} \geq 0.3 \quad (35)$$

in which

$$\lambda_{fc} = 0.75 + 0.008 f_{c0} \quad (f_{c0} \text{ in MPa}) \quad (36)$$

$$\lambda_{Rf} = 1 + 0.5 R_f \quad (37)$$

$$\lambda_D = 0.82 + 0.0012 D \geq 1 \quad (D \text{ in MPa}) \quad (38)$$

where λ_{fc} , λ_{Rf} and λ_D are the calibration terms introduced to reflect the influence of f_{c0} , R_f and D in Eq. (34). To highlight the correlations of Eqs. (34 and 35), the developed R_1 and R_2 were compared to the extracted experimental results in Fig. 10. The statistical indicators show that the proposed equations for these parameters estimate the experimental counterparts of FFC/FPC with acceptable accuracy. It should be noted that since the proposed confinement model was developed with a uniform approach for FFC and FPC, Eq. (33) can be considered

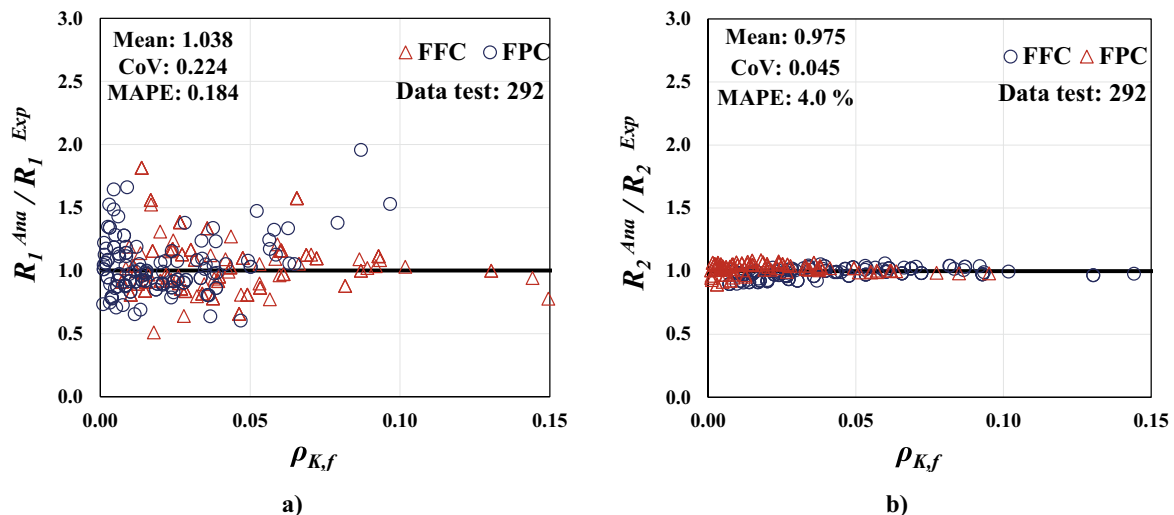


Fig. 10. Test data and regression equations for: a) R_1 , and b) R_2 .

valid for both cases. The incremental calculation procedure based on the developed model to determine the axial response of FFC/FPC with ρ_{Kf} is as follows:

- 1- Assume a value of ϵ_c .
- 2- Calculate the secant Poisson's ratio v_s as a function of ρ_{Kf} (from Fig. 8 considering Eqs. (26–28)).
- 3- Calculate the peak axial stress f_{cc} using Eq. (33).
- 4- Calculate the peak axial stress ϵ_{cc} using Eq. (30).
- 5- Calculate the axial stress f_c using Eq. (29).
- 6- Continue the steps 1–5 up to ultimate condition.

6. Ultimate condition

In this section, a new methodology will be introduced to determine ultimate axial strain of FFC and FPC under axial compressive loading. According to failure mechanism of FFC (Fig. 11a), when the maximum concrete hoop strain along the column height reaches FRP ultimate hoop strain ($\epsilon_{h,rupt}$), the confinement provided by the FRP is lost, followed by an abrupt column's load decay. However, in the case of FPC with a large s_f , damage tends to initiate by concrete spalling, and the specimen finally fails as concrete crushing along with inclined concrete cracking between FRP strips, as illustrated in Fig. 11e. In this case, as concrete lateral expansion at the critical section increases, FRP hoop strain at the mid-plane of the strips, generating lateral confinement, does not enhance considerably due to lower concrete expansion. Accordingly, the failure mechanism can be regarded as that of unconfined concrete. However, by decreasing s_f , since expansion at the mid-plane of the strips would increase, the confined column would fail due to rupture of FRP jacket (Fig. 11b-d). According to the failure mechanism of partially confined columns, concrete lateral expansion increases until hoop rupture of FRP jacket along with concrete crushing simultaneously. The concrete crushing seems to be more probable in the case of the specimens with larger R_f due to a substantial increase in ineffective confinement area.

In this study, for the calculation of the ultimate axial strain (ϵ_{cu}), a unified model with a design framework was developed applicable to both cases of FFC and FPC based on a combination of theoretical basics and regression analysis. For the case of FFC, when maximum hoop strain ($\epsilon_{h,max}$) in FRP jacket reaches FRP hoop rupture strain, $\epsilon_{h,rupt}$, the corresponding $v_{s,u}$ depending on $\epsilon_{cu} = \epsilon_{cu,r}$ can be determined as:

$$v_{s,u} = \frac{\epsilon_{h,max}}{\epsilon_{cu,r}} = \frac{\epsilon_{h,rupt}}{\epsilon_{cu,r}} \quad (39)$$

By defining $\epsilon_{h,rupt} = \beta_\epsilon \epsilon_{fu}$ and $v_{s,u} = \alpha_v v_{s,max}$, then rearranging Eq. (39), the normalized ultimate axial strain can be expressed as:

$$\frac{\epsilon_{cu,r}}{\epsilon_{c0}} = \frac{\epsilon_{h,rupt}}{v_{s,u} \epsilon_{c0}} = \frac{\beta_\epsilon \epsilon_{fu}}{\alpha_v v_{s,max} \epsilon_{c0}} = \frac{\beta_\epsilon \rho_\epsilon}{\alpha_v v_{s,max}} \quad (40)$$

in which

$$\rho_\epsilon = \frac{\epsilon_{fu}}{\epsilon_{c0}} \quad (41)$$

where α_v is the ratio of $v_{s,u}$ and $v_{s,max}$; β_ϵ introduces the ratio of FRP ultimate hoop strain ($\epsilon_{h,rupt}$) and FRP ultimate tensile strain (ϵ_{fu}). To obtain the α_v , the ratio of $v_{s,u}$ at $\epsilon_{cu,r}^{Exp}$ and $v_{s,max}$ for 191 test specimens of FFC were simulated by the developed dilation model, and the obtained results are presented in Fig. 12a. By best fitting these results, the following equation was obtained:

$$\alpha_v = 1 - 0.85 \rho_{Kf} \geq 0.8 \quad (42)$$

It should be noted that in Eq. (42), for low level of ρ_{Kf} ($\rho_{Kf} \leq 0.015$) (with $\epsilon_{cu,r}^{Exp} < \epsilon_{c,m}$), the ascending branch α_v versus ρ_{Kf} relation was neglected for the sake of simplification. Then, by using Eq. (42), β_ϵ^{Exp} was calculated as $\alpha_v v_{s,max} \epsilon_{cu,r}^{Exp} / \epsilon_{fu}$. Accordingly, the relation of β_ϵ with f_{c0} was determined as follows (Fig. 12b):

$$\beta_\epsilon = 1.45 f_{c0}^{-0.27} \quad (43)$$

Therefore, with the consideration of $v_{s,max} = 0.15 / \sqrt{\rho_{Kf}}$ (Fig. 9a), replacing Eq. (43) in Eq. (40) leads to:

$$\frac{\epsilon_{cu,r}}{\epsilon_{c0}} = 9.67 f_{c0}^{-0.27} \frac{\sqrt{\rho_{Kf}}}{1 - 0.85 \rho_{Kf}} \rho_\epsilon \quad (44)$$

In order to simplify Eq. (44), rearranging this equation gives:

$$\frac{\epsilon_{cu,r}}{X} = \frac{\sqrt{\rho_{Kf}}}{1 - 0.85 \rho_{Kf}} \approx C_1 \rho_{Kf}^{C_2} \quad (45)$$

in which $X = 9.67 f_{c0}^{-0.27} \epsilon_{c0} \rho_\epsilon$, while C_1 and C_2 are the calibration factors, which were determined equal to 1.83 and 0.61, respectively, based on the relation of $\epsilon_{cu,r} / X$ with ρ_{Kf} as demonstrated in Fig. 13c. Accordingly, $\epsilon_{cu,r}$ can be expressed as:

$$\frac{\epsilon_{cu,r}}{\epsilon_{c0}} = 17.7 f_{c0}^{-0.27} \rho_{Kf}^{0.61} \rho_\epsilon \geq 1.5 \quad (46)$$

The lower bound of 1.5 was considered to limit ultimate axial strain corresponding to unconfined concrete. For the case of FPC, $\epsilon_{cu,r}$ corresponding to $\epsilon_{h,rupt} = k_{ff}^{FPC} \epsilon_{ij}$ at the FRP strips can be written as:

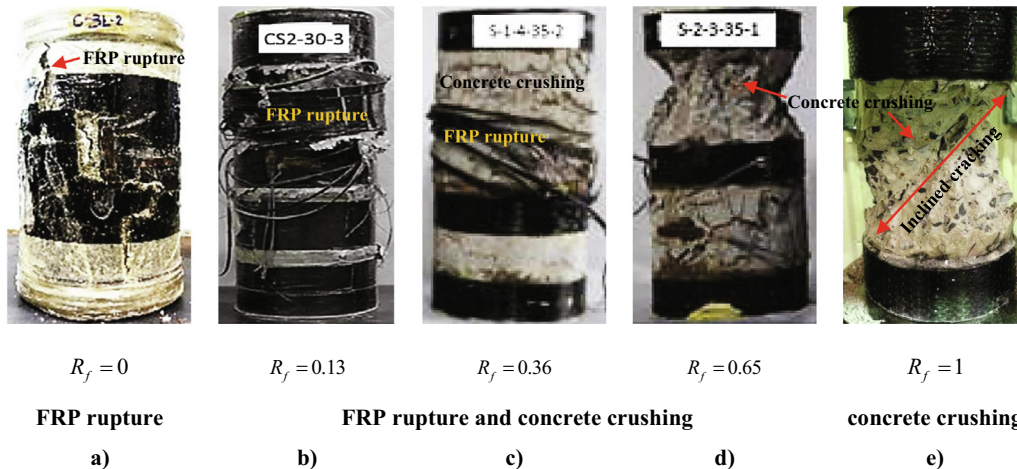


Fig. 11. Failure mechanisms of FRP confined concrete based on the experimental studies conducted by a) Suon et al. [45]; b) Zeng et al. [43]; c, d) Zeng et al. [5]; e) Wang et al. [44].

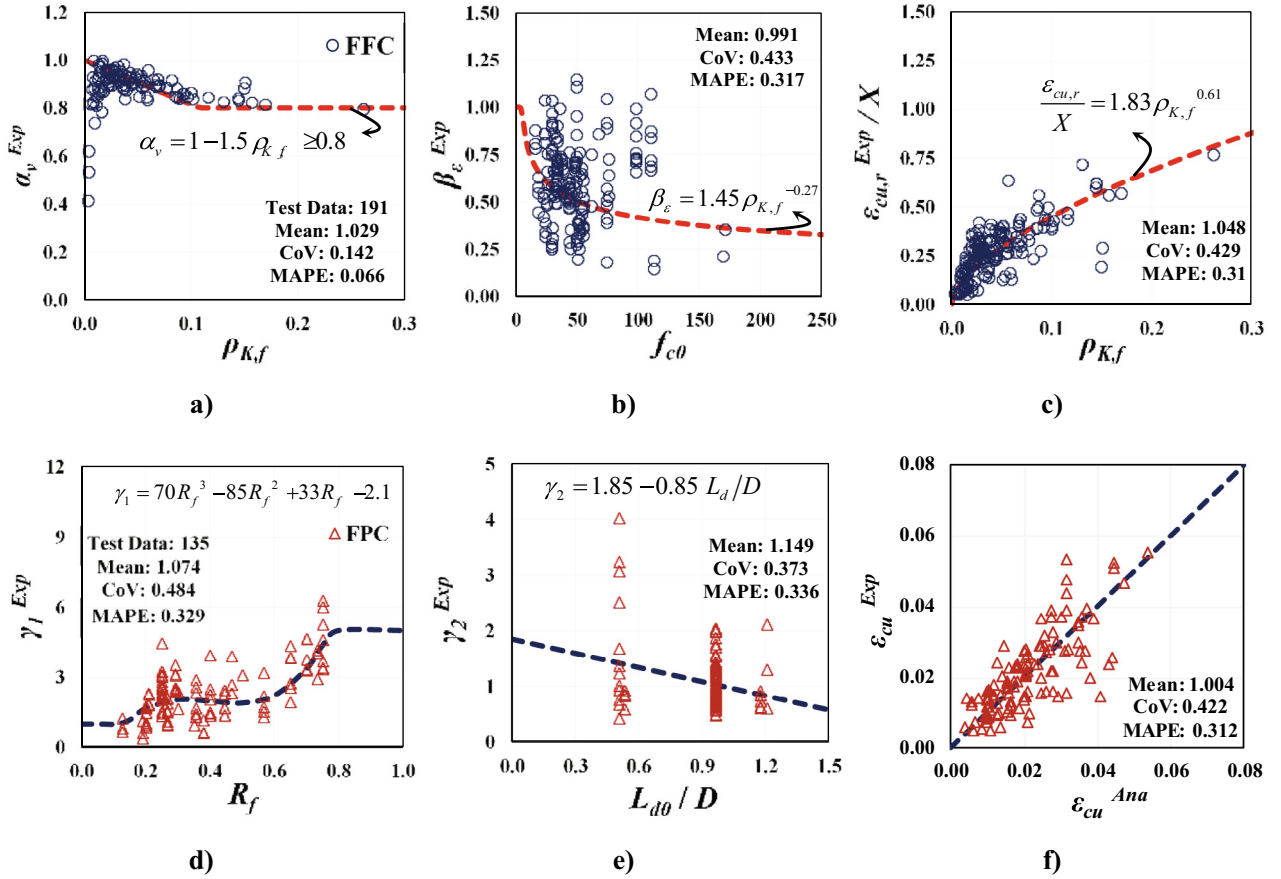


Fig. 12. Comparison of experimental results and analytical models.

$$\epsilon_{cu,r} = \frac{\epsilon_{lj}}{v_{s,u}} = \frac{\epsilon_{h,rupt}}{K_{ff}^{FPC} v_{s,u}} \quad (47)$$

Rearranging Eq. (38), the normalized ultimate axial strain can be expressed as:

$$\frac{\epsilon_{cu,r}}{\epsilon_{c0}} = \frac{\epsilon_{h,rupt}}{K_{ff}^{FPC} v_{s,u} \epsilon_{c0}} = \frac{\beta_\epsilon \rho_\epsilon}{K_{ff}^{FPC} \alpha_v v_{s,max}} = \frac{17.7}{K_{ff}^{FPC}} f_{c0}^{-0.27} \rho_{K,f}^{0.61} \rho_\epsilon \quad (48)$$

In order to minimize the complexity of Eq. (48), based on the best-fit with the derived results from 135 test specimens of FPC, Eq. (48) was simplified as follows:

$$\frac{\epsilon_{cu,r}}{\epsilon_{c0}} = 17.7 \gamma_{sf} f_{c0}^{-0.27} \rho_{K,f}^{0.61} \rho_\epsilon \ge 1.5 \quad (f_{c0} \text{ in MPa}) \quad (49)$$

in which

$$\gamma_{sf} = \frac{\gamma_1}{\gamma_2} \quad (50)$$

$$\gamma_1 = 70R_f^3 - 85R_f^2 + 33R_f - 2.1 \le 5 \quad (51)$$

$$\gamma_2 = 1.85 - 0.85 \frac{L_{d0}}{D} \quad (52)$$

where γ_{sf} , γ_1 and γ_2 are the calibration parameters determined based on regression analyses as shown in Fig. 12d-e; R_f defines the ratio of the FRP strip distance (s_f) and the column cross-section diameter (D) as presented in Eq. (15). It should be noted that γ_1^{Exp} and γ_2^{Exp} were determined based on Eq. (49), as $\gamma_1^{Exp} = \epsilon_{cu,r}^{Exp} / (17.7 f_{c0}^{-0.27} \rho_{K,f}^{0.61} \rho_\epsilon \epsilon_{c0})$ and $\gamma_2^{Exp} = (17.7 \gamma_1 f_{c0}^{-0.27} \rho_{K,f}^{0.61} \rho_\epsilon \epsilon_{c0}) / \epsilon_{cu,r}^{Exp}$, respectively.

For the case of FPC with a large R_f , the failure mode is prominently overwhelmed by the concrete crushing within the damage length zone. Wang et al. [44] experimentally evidenced that for the case of $R_f \geq 1$, the failure mode would be as concrete crushing with no FRP rupture (Fig. 11e). It can be attributed to the difference in Poisson's ratio at the critical section experiencing a major damage and at the mid-plane of FRP strip in which concrete expansion could not be enough to increase FRP hoop strain to experience the rupture. Accordingly, for FPC with a large R_f , the application of Eq. (49), predicting ultimate axial strain corresponding to FRP rupture ($\epsilon_{cu,r}$), might lead to overestimation in terms of deformability, considering the fact that FPC would behave similar to unconfined concrete. Shayanfar et al. [23] developed a new methodology to predict ultimate axial strain (ϵ_{cu}) of FPC formulating the possibility of concrete crushing failure mode ($\epsilon_{cu,c}^{FPC}$), in addition to FRP rupture ($\epsilon_{cu,r}$), leading to $\epsilon_{cu} = \min(\epsilon_{cu,r}, \epsilon_{cu,c}^{FPC})$. Since all test specimens of FFC with $R_f \leq 0.75$, available in the test database, experienced FRP rupture failure mode, the application of $\epsilon_{cu,r}$ in Eq. (49) for estimation of ϵ_{cu} would be reasonable. However, for the case of $R_f \geq 0.75$, based on Shayanfar et al. [23], an upper bound needs to be introduced to restrain ultimate axial strain by considering the possibility of concrete crushing. Even though the application of FPC with $R_f \geq 0.75$ is not allowed in the real strengthening cases, in the present study, ϵ_{cu} for $R_f \geq 0.75$ was assumed to be equal to $\epsilon_{cu,r}$ and $1.5\epsilon_{c0}$ (ultimate axial strain of unconfined concrete) corresponding to $R_f = 0.75$ and $R_f \geq 1$ (considered as unconfined concrete), respectively. Consequently, using a linear function, $\epsilon_{cu,c}^{FPC}$ can be as determined as:

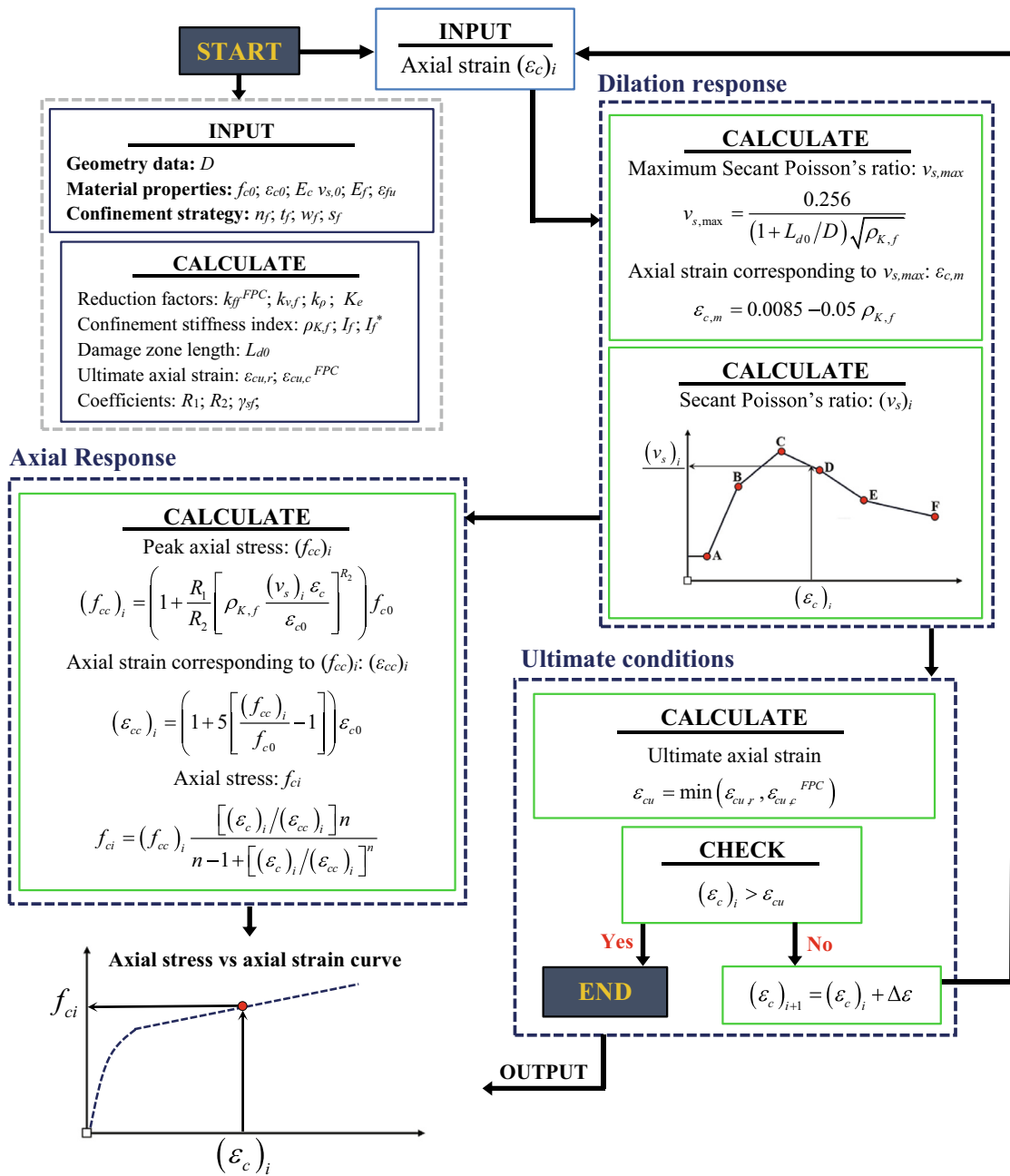


Fig. 13. A flowchart for calculating the characteristics of FFC/FPC.

$$\frac{\epsilon_{cu,c}^{FPC}}{\epsilon_{c0}} = 1.5 + 4 \left(\frac{\epsilon_{cu,r}}{\epsilon_{c0}} - 1.5 \right) (1 - R_f) \geq 1.5 \quad (53)$$

In Fig. 12f, ultimate axial strains of FPC obtained from the developed model were compared with those of the experimental studies. It can be evidenced that the proposed approach is capable of calculating ϵ_{cu} ($\min(\epsilon_{cu,r}, \epsilon_{cu,c}^{FPC})$) with an acceptable agreement with the experimental counterparts.

7. Verification

In this section, the reliability of the proposed confinement model in simulating the experimental counterparts is addressed. In Fig. 13, a flowchart for calculating axial stress–strain curve of FRP fully/partially

confined concrete columns is presented. As can be seen, the effectiveness of FRP confining system can be easily determined through following the proposed incremental procedure. In order to appropriately assess the model, in addition to global axial response, its capability in predicting the dilation response is also examined. Zeng et al. [5] conducted an experimental study on fully/partially FRP confined circular concrete with different s_f , n_f and confinement types of full and partial systems. The test specimens had a diameter of 150 mm with a height of 300 mm. The compressive strength of unconfined cylindrical concrete was 23.4 MPa. The values of thickness, tensile elastic modulus and rupture strain of FRP strips were reported as 0.167 mm, 249.1 GPa and 1.66%, respectively. Complete detailed of the test specimens can be found from Zeng et al. [5]. The axial and dilation responses of the test specimens reported by the experiment

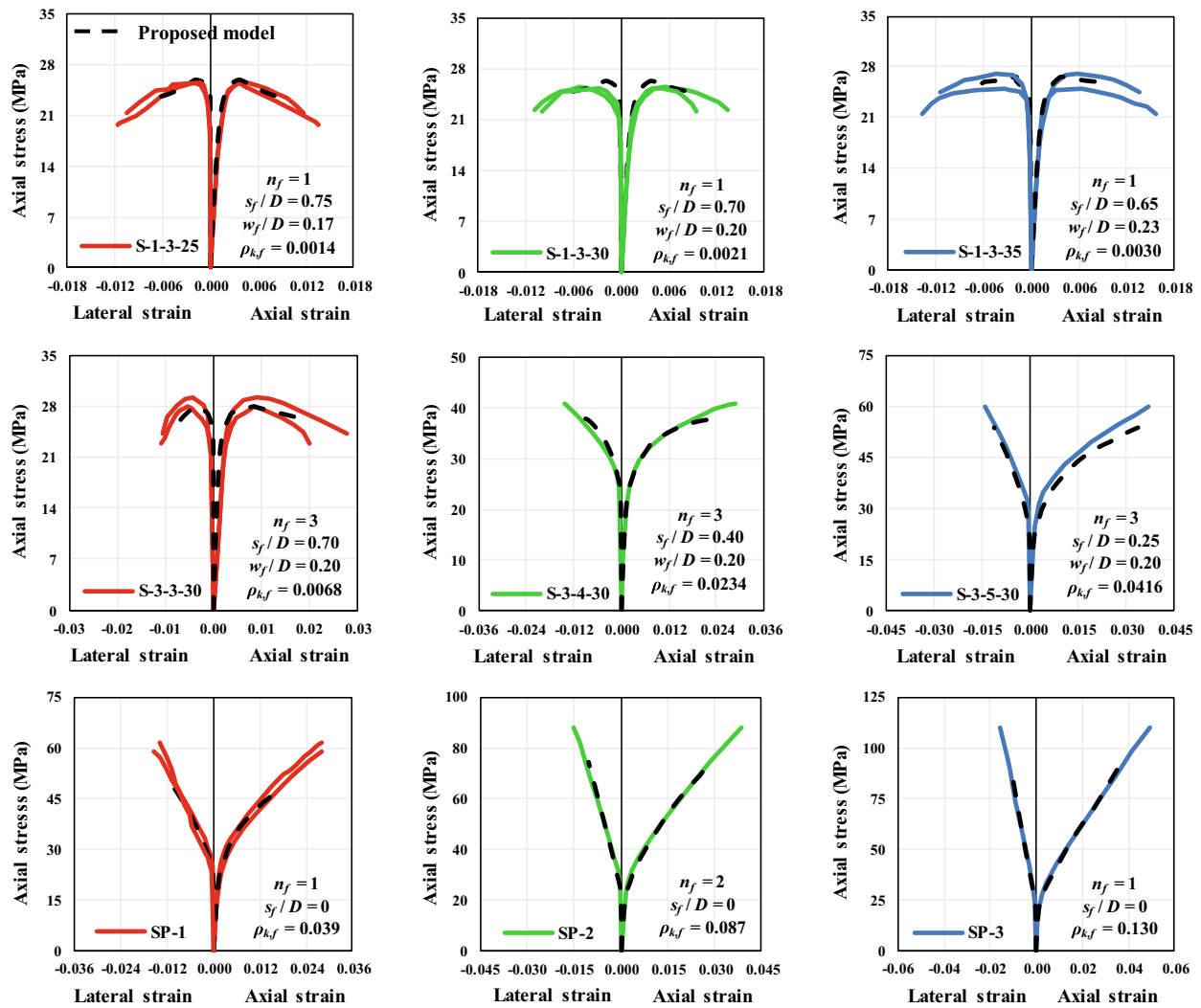


Fig. 14. Analytical analysis versus experimental results for the FRP fully/partially confined specimens tested by Zeng et al. [5].

and obtained from the proposed model are compared in Fig. 14. As can be observed, the proposed model has a good predictive performance, with a slightly conservative tendency to predict not only the global axial stress–strain curves of the test specimens with full/partial confinement systems, but also experimental axial stress versus lateral strain.

For further examination of the model capability in predicting axial response, In Fig. 15, axial responses obtained from the analytical model are compared to those experimentally measured by Zeng et al. [43], Shan et al. [46] and Gue et al. [8], which are the larger dimension specimens found in the database for the assessment of the performance of the developed model in predicting their axial stress–strain response. As can be seen, the predictions are in an acceptable agreement with the global axial stress–strain curve of the experimental FFC/FPC specimens. Supplementary results regarding the validations of the developed model in simulating axial behavior of FFC and FPC can be found, respectively, in Figs. B1 and B2 in Appendix B.

Fig. 16 evaluated the predictive performance of the developed confinement model, in the estimation of ultimate axial stress and strain (f_{cu}^{Exp} and ϵ_{cu}^{Exp}) of FFC and FPC, compared to that of existing models recommended by fib [25], CNR DT 200/2004 [26] and ACI 440.2R-17 [27], which can be found in Appendix A.

As can be seen, for the case of FFC, the proposed model provided the most accurate and uniform predictions of f_{cu}^{Exp} with the values of mean, SD (standard deviation) and MAPE (mean absolute percentage error) which is expressed as $MAPE = 1/N \sum_{i=1}^N |1 - f_{cu}^{Ana} / f_{cu}^{Exp}|$ where N is the total number of the test data) as 0.99, 0.15 and 0.12, respectively. ACI 440.2R-17 [27] presented a slight underestimation of the experimental counterpart (mean = 0.89), with the values of SD and MAPE as 0.15 and 0.15. On the other hand, for the case of FPC, CNR DT 200/2004 [26] demonstrated the most accurate model, with the values of mean, SD and MAPE as 1.00, 0.12 and 0.10, respectively. The predictive performance of the proposed model in predicting f_{cu}^{Exp} is virtually identical to CNR DT 200/2004 [26], but with slightly more SD equal to 0.13.

For the case of ϵ_{cu}^{Exp} , fib [25] and CNR DT 200/2004 [26] conservatively predicted the experimental counterparts, even though ACI 440.2R-17 [27] seems to provide better estimations of ultimate axial strain for the case of FFC, non-conservative results for some test specimens of FPC are obtained which slightly overwhelm its reliability evaluation. The predictive performance of Eq. (48) confirmed its reliability to predict the experimental axial strain with sufficient accuracy demonstrated by the relative statistical values for the both cases of FFC and FPC.

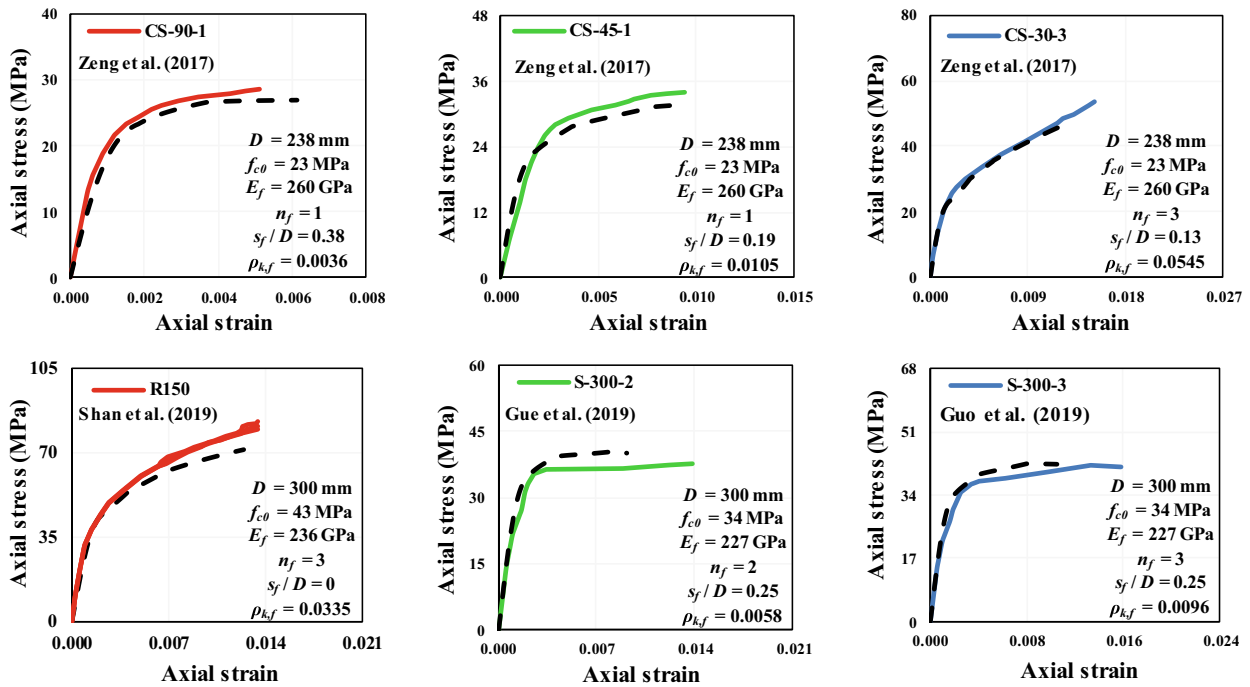


Fig. 15. Analytical analysis versus experimental results for FFC/FPC specimens tested by Zeng et al. [43], Shan et al. [46], and Gue et al. [8].

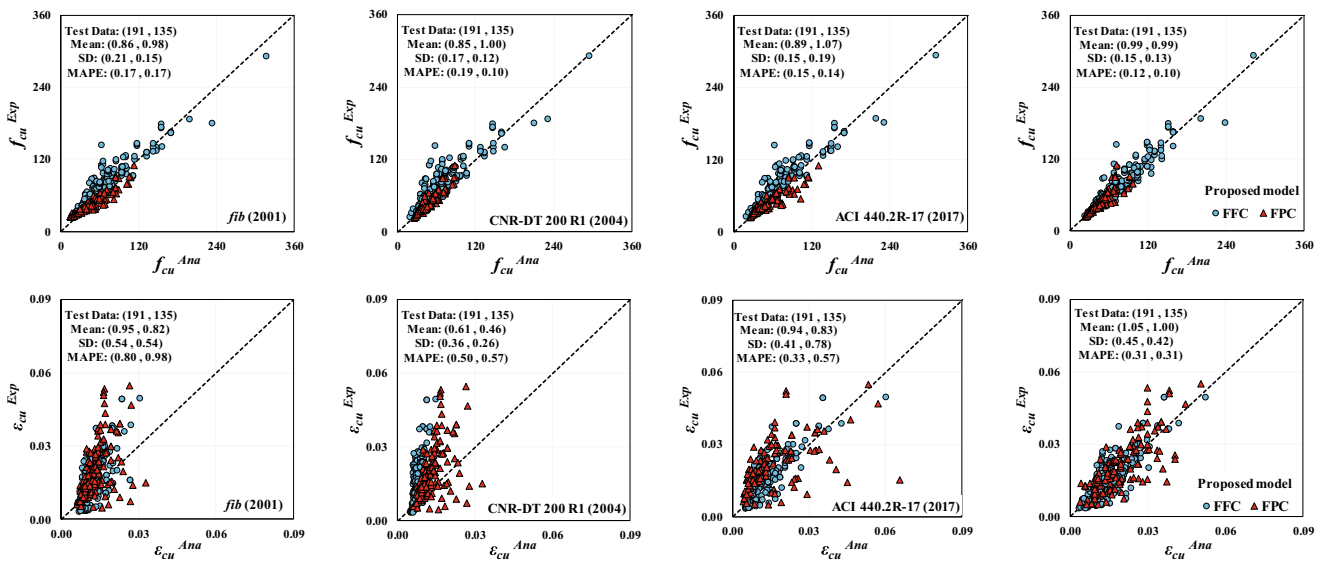


Fig. 16. Comparison of experimental results and analytical models.

As demonstrated in Figs. 14-16, it can be concluded that the developed model conducted in the present study is sufficiently capable of predicting not only the global axial stress–strain relationship of FFC/FPC, but also the ultimate conditions (f_{cu}^{Exp} and ϵ_{cu}^{Exp}).

8. Summary and conclusions

In the present study, a new unified confinement model applicable to different confinement scenarios including circular cross-sections concrete columns with full and partial confining strategies was proposed. To simulate the axial stress versus strain curve, a new strength model is proposed addressing the relation of axial stress and confine-

ment pressure during axial loading, whose calibration was based on an extensive set of test results. For formulating the influence of concrete expansion distribution in the calculation of confinement pressure, Shayanfar et al. [23]’s model is extended to be applicable to FFC as a function of confinement stiffness, along with some refinements for the case of FPC. In this model, the concrete lateral expansibility was addressed as a main function of confinement stiffness (I_f) and also s_f/L_{d0} for the case of FPC. A new expression is subsequently developed to estimate ultimate axial strain of FFC/FPC with a combination of theoretical basis and experimental observations. Lastly, the predictive performance of the developed confinement model was assessed through analytically simulating experimental counterparts.

The comparison between the analytical model and experimental counterparts demonstrated that global axial stress–strain curves simulated by the proposed confinement model are in good agreement with those registered experimentally in available literature, and provides better predictions in terms of ultimate axial stress/strain than the formulations proposed by design standards. The authors are working on the extension of the present formulation in order to be applicable to non-circular cross section columns, where the non-homogeneous concrete expansibility at the cross-section level must be also considered by taking into account the influence of the sectional corner radius.

9. Data Availability Statement

All data and models related to the present study could be available from the corresponding author upon rational request.

CRediT authorship contribution statement

Javad Shayanfar: Conceptualization, Methodology, Data curation, Validation, Writing - original draft. **Joaquim A.O. Barros:** Conceptualization, Methodology, Writing - review & editing, Supervision. **Mohammadali Rezazadeh:** Conceptualization, Methodology, Data curation, Writing - review & editing.

Declaration of Competing Interest

The authors declare that they have no known competing financial interests or personal relationships that could have appeared to influence the work reported in this paper.

Acknowledgment

This study is a part of the project “StreColesf_Innovative technique using effectively composite materials for the strengthening of rectangular cross section reinforced concrete columns exposed to seismic loadings and fire”, with the reference POCI-01-0145-FEDER-029485. The first author also acknowledges the support provided by FCT PhD individual fellowship 2019 with the reference of “SFRH/BD/148002/2019”.

Appendix A

In this section, a brief description of the confinement models recommended by fib [25], CNR DT 200/2004 [26] and ACI 440.2R-17 [27] will be introduced for predicting the ultimate axial strain and the ultimate axial stress of concrete.

fib [25]

$$\frac{f_{cu}}{f_{c0}} = 0.3 + 3\sqrt{\frac{f_{l,eff}}{f_{c0}}} \tag{A-1}$$

$$\frac{\epsilon_{cu}}{\epsilon_{c0}} = 2 + 1.25 \frac{E_c \epsilon_{h,rupt}}{f_{c0}} \sqrt{\frac{f_{l,eff}}{f_{c0}}} \tag{A-2}$$

CNR DT 200/2004 [26]

$$\frac{f_{cu}}{f_{c0}} = 1 + 2.6 \left(\frac{f_{l,eff}}{f_{c0}} \right)^{\frac{2}{3}} \tag{A-3}$$

$$\frac{\epsilon_{cu}}{\epsilon_{c0}} = 0.0035 + 0.015 \sqrt{\frac{f_{l,eff}}{f_{c0}}} \tag{A-4}$$

ACI 440.2R-17 [27]

$$\frac{f_{cu}}{f_{c0}} = 1 + 3.3\psi_f \frac{f_{l,eff}}{f_{c0}} \tag{A-5}$$

$$\frac{\epsilon_{cu}}{\epsilon_{c0}} = 1.75 + 12 \frac{f_{l,eff}}{f_{c0}} \left(\frac{\epsilon_{h,rupt}}{\epsilon_{c0}} \right)^{0.45} \tag{A-6}$$

where E_c is the concrete modulus elasticity; $\epsilon_{h,rupt}$ is the effective hoop strain at FRP rupture; ψ_f is the additional reduction factor, equal to 0.95; $f_{l,eff}$ defines the effective confinement pressure of FPC, recommended by

$$f_{l,eff} = k_{v,f} f_{l,f} = \frac{1}{2} k_{v,f} \rho_f E_f \epsilon_{h,rupt} \tag{A-7}$$

in which

$$\epsilon_{h,rupt} = \beta_\epsilon \epsilon_{fu} \tag{A-8}$$

$$k_{v,f} = \left(1 - \frac{s_f}{2D} \right)^2 \tag{A-9}$$

where ρ_f is the FRP volumetric ratio; E_f is the FRP modulus elasticity; $k_{v,f}$ is the confinement efficiency factor; β_ϵ is FRP efficiency factor; and ϵ_{fu} is the ultimate FRP tensile strain.

Appendix B

The axial and dilation responses of the test specimens of FFC conducted by Lim and Ozbakkaloglu [4] and FPC tested by Barros and Ferreira [6], Zeng et al. [7] and Gue et al. [8] are compared with those obtained from the proposed model in Figs. B1 and B2, respectively.

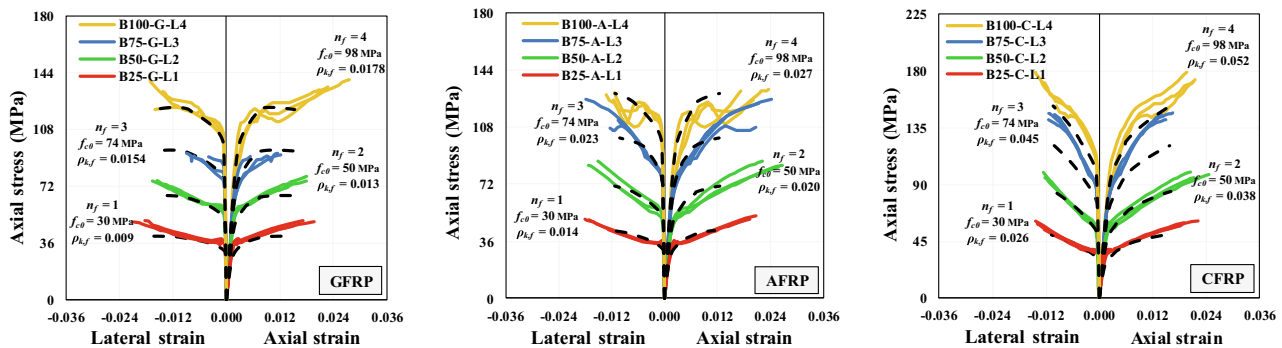


Fig. B1. Analytical analyses versus experimental results for FFC specimens tested by Lim and Ozbakkaloglu [4].

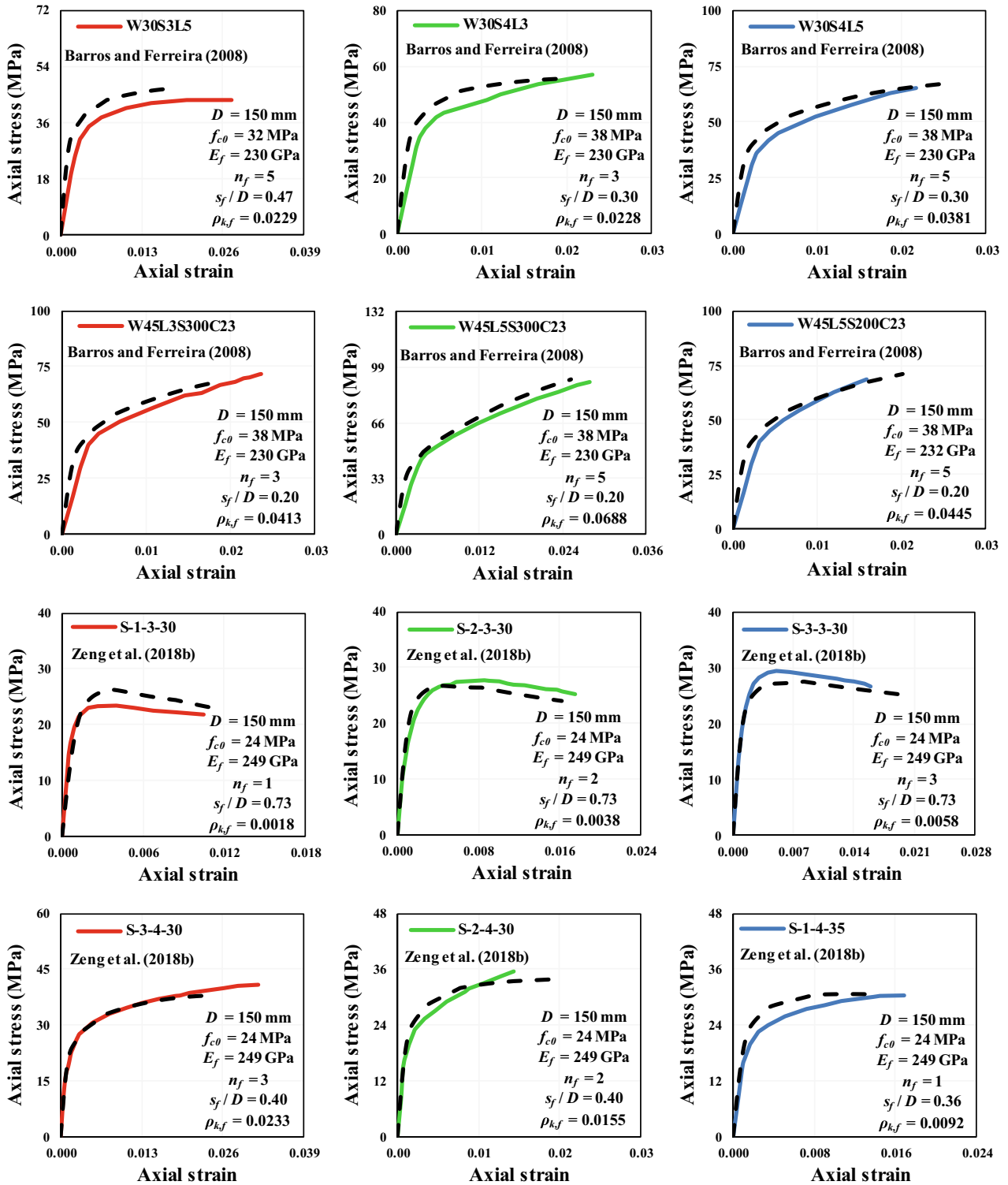


Fig. B2. Analytical analysis versus experimental results for FPC specimens tested by Barros and Ferreira [6], Zeng et al. [7] and Gue et al. [8].

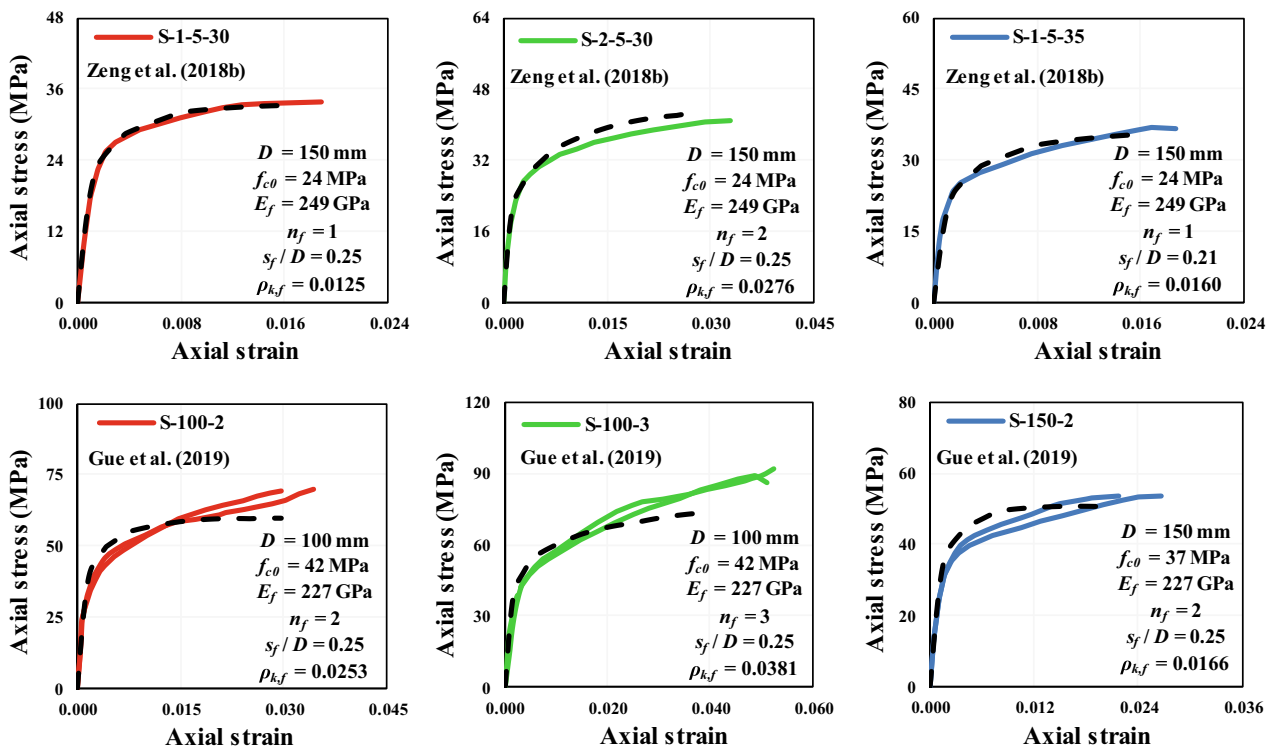


Fig. B2 (continued)

References

- [1] De Oliveira DS, Raiz V, Carrazedo. Experimental study on normal-strength, high-strength and ultrahigh-strength concrete confined by carbon and glass FRP laminates. *J Compos Constr* 2019;23(1):04018072.
- [2] Lim JC, Ozbakkaloglu T. Lateral strain-to-axial strain relationship of confined concrete. *J Struct Eng* 2014;141(5):04014141.
- [3] Lim JC, Ozbakkaloglu T. Unified stress-strain model for FRP and actively confined normal strength and high-strength concrete. *J Compos Constr* 2014;19(4):04014072.
- [4] Lim JC, Ozbakkaloglu T. Hoop strains in FRP-confined concrete columns: experimental observations. *Mater Struct* 2014;48(9):2839–54.
- [5] Zeng JJ, Guo YC, Gao WY, Chen WP, Li LJ. Stress-strain behavior of concrete in circular concrete columns partially wrapped with FRP strips. *Compos Struct* 2018;200:810–28.
- [6] Barros JA, Ferreira DR. Assessing the efficiency of CFRP discrete confinement systems for concrete cylinders. *J Compos Constr* 2008;12(2):134–48.
- [7] Zeng JJ, Guo YC, Li L, Chen W. Behavior and three-dimensional finite element modeling of circular concrete columns partially wrapped with FRP strips. *Polymers* 2018;10(3):253.
- [8] Guo YC, Gao WY, Zeng JJ, Duan ZJ, Ni XY, Peng KD. Compressive behavior of FRP ring-confined concrete in circular columns: Effects of specimen size and a new design-oriented stress-strain model. *Constr Build Mater* 2019;201:350–68.
- [9] Guo YC, Xiao SH, Luo JW, Ye YY, Zeng JJ. Confined concrete in fiber-reinforced polymer partially wrapped square columns: axial compressive behavior and strain distributions by a particle image velocimetry sensing technique. *Sensors* 2018;18(12):4118.
- [10] Janwaen W, Barros JA, Costa IG. A new strengthening technique for increasing the load carrying capacity of rectangular reinforced concrete columns subjected to axial compressive loading. *Compos Part B Eng* 2019;158:67–81.
- [11] Janwaen W, Barros JA, Costa IG. New hybrid FRP Strengthening technique for rectangular RC columns subjected to eccentric compressive loading. *J Compos Constr* 2020;24(5):04020043.
- [12] Jiang T, Teng JG. Analysis-oriented stress-strain models for FRP-confined concrete. *Eng Struct* 2007;29(11):2968–86.
- [13] Teng J, Huang YL, Lam L, Ye LP. Theoretical model for fiber-reinforced polymer-confined concrete. *J Compos Constr* 2007;11(2):201–10.
- [14] Teng JG, Lin G, Yu T. Analysis-oriented stress-strain model for concrete under combined FRP-steel confinement. *J Compos Constr* 2015;19(5):04014084.
- [15] Lim JC, Ozbakkaloglu T. Stress-strain model for normal-and light-weight concretes under uniaxial and triaxial compression. *Constr Build Mater* 2014;71:492–509.
- [16] Popovics S. A numerical approach to the complete stress-strain curve of concrete. *Cem Concr Res* 1973;3(5):583–99.
- [17] Lin S, Zhao YG, Li J, Lu ZH. Confining stress path-based compressive strength model of axially loaded FRP-confined columns. *J Compos Constr* 2020;25(1):04020077.
- [18] Yang JQ, Feng P. Analysis-oriented models for FRP-confined concrete: 3D interpretation and general methodology. *Eng Struct* 2020;216:110749.
- [19] Zhao YG, Lin S, Lu ZH, Saito T, He L. Loading paths of confined concrete in circular concrete loaded CFT stub columns subjected to axial compression. *Eng Struct* 2018;156:21–31.
- [20] Wu YF, Wei Y. Stress-strain modeling of concrete columns with localized failure: an analytical study. *J Compos Constr* 2016;20(3):04015071.
- [21] Wei Y, Wu YF. Experimental study of concrete columns with localized failure. *J Compos Constr* 2016;20(5):04016032.
- [22] Fallahpour A, Nguyen GD, Vincent T, Ozbakkaloglu T. Investigation of the compressive behavior and failure modes of unconfined and FRP-confined concrete using digital image correlation. *Compos Struct* 2020;252:112642.
- [23] Shayanfar J, Rezazadeh M, Barros JA. Analytical model to predict dilation behavior of FRP confined circular concrete columns subjected to axial compressive loading. *J Compos Constr* 2020;24(6):04020071.
- [24] Mander JB, Priestley MJ, Park R. Theoretical stress-strain model for confined concrete. *J Struct Eng* 1988;114(8):1804–26.
- [25] Fib Bulletin 14. Externally bonded FRP reinforcement for RC structures. International Federation for Structural Concrete 2001.
- [26] CNR-DT 200. Guide for the design and construction of externally bonded FRP systems for strengthening existing structures. Italian National Research Council 2004.
- [27] ACI 440.2R-17. Guide for the design and construction of externally bonded FRP systems for strengthening concrete structures; American Concrete Institute (ACI): Farmington Hills MI USA 2017.
- [28] Teng JG, Jiang T, Lam L, Luo YZ. Refinement of a design-oriented stress-strain model for FRP-confined concrete. *J Compos Constr* 2010;13(4):269–78.
- [29] Karthik MM, Mander JB. Stress-block parameters for unconfined and confined concrete based on a unified stress-strain model. *J Struct Eng* 2010;137(2):270–3.
- [30] Wang LM, Wu YF. Effect of corner radius on the performance of CFRP-confined square concrete columns: test. *Eng Struct* 2008;30(2):493–505.
- [31] Eid R, Roy N, Paultre P. Normal-and high-strength concrete circular elements wrapped with FRP composites. *J Compos Constr* 2009;13(2):113–24.
- [32] Shayanfar J, Rezazadeh M, Barros JA, Ramezansafat H. A new dilation model for FRP fully/partially confined concrete column under axial loading. The 3RD RILEM Spring Convention 2020 Ambitioning a Sustainable Future for Built Environment. Guimarães Portugal: Comprehensive Strategies for Unprecedented Challenges; 2020.
- [33] Lertsrisakulrat T, Watanabe K, Matsuo M, Niwa J. Experimental study on parameters in localization of concrete subjected to compression. *J Mater Concr Struct Pavements* 2001;50(669):309–21.

- [34] Candappa DC, Sanjayan JG, Setunge S. Complete triaxial stress-strain curves of high-strength concrete. *J Mater Civ Eng* 2001;13(3):209–15.
- [35] Rochette P, Labossiere P. Axial testing of rectangular column models confined with composites. *J Compos Constr* 2000;4(3):129–36.
- [36] Shehata IA, Carneiro LA, Shehata LC. Strength of short concrete columns confined with CFRP sheets. *Mater Struct* 2002;35(1):50–8.
- [37] Teng JG, Lam L. Compressive behavior of carbon fiber reinforced polymer-confined concrete in elliptical columns. *J Struct Eng* 2002;128(12):1535–43.
- [38] Xiao Y, Wu H. Compressive behavior of concrete confined by various types of FRP composite jackets. *J Reinforc Plast Compos* 2003;22(13):1187–201.
- [39] Berthet JF, Ferrier E, Hamelin P. Compressive behavior of concrete externally confined by composite jackets. Part A: experimental study. *Constr Build Mater* 2005;19(3):223–32.
- [40] Wang F, Wu HL. Size effect of concrete short columns confined with aramid FRP jackets. *J Compos Constr* 2011;15(4):535–44.
- [41] Benzaid R, Mesbah HA. Circular and square concrete columns externally confined by CFRP composite: experimental investigation and effective strength models. *Fiber Reinforced Polymers—The Technology Applied for Concrete Repair* 2013;167–201.
- [42] Vincent T, Ozbakkaloglu T. Compressive behavior of prestressed high-strength concrete-filled aramid FRP tube columns: experimental observations. *J Compos Constr* 2015;19(6):04015003.
- [43] Zeng JJ, Guo YC, Gao WY, Li JZ, Xie JH. Behavior of partially and fully FRP-confined circularized square columns under axial compression. *Constr Build Mater* 2017;152:319–32.
- [44] Wang W, Sheikh MN, Al-Baali AQ, Hadi MN. Compressive behaviour of partially FRP confined concrete: experimental observations and assessment of the stress-strain models. *Constr Build Mater* 2018;192:785–97.
- [45] Suon S, Saleem S, Pimanmas A. Compressive behavior of basalt FRP-confined circular and non-circular concrete specimens. *Constr Build Mater* 2019;19, :85–103.
- [46] Shan B, Gui FC, Monti G, Xiao Y. Effectiveness of CFRP confinement and compressive strength of square concrete columns. *J Compos Constr* 2019 23 (6):04019043.
- [47] Carreira, Chu. Stress-strain relationship for plain concrete in compression. In *Journal Proceedings* 1985;82(6):797–804.